1

Measurement of Microwave Dielectric Properties and Factors Affecting Them

M.T. Sebastian,[1] M.A.S. Silva,[2] and A.S.B. Sombra[2]
[1]Microelectronics Research Unit, Faculty of Information Technology and Electrical Engineering, University of Oulu, Oulu, Finland
[2]LOCEM–Laboratory of Telecommunications and Materials Science and Engineering, Physics Department, Federal University of Ceará (UFC), Ceará, Brazil

1.1 Introduction

Recently extensive researches have been done on microwave materials such as dielectric resonators (DR), electromagnetic interference (EMI) shielding materials, tunable dielectrics, high-temperature cofired ceramics (HTCC), low-temperature cofired ceramics (LTCC), polymer or rubber–ceramic composites, dielectric inks, microwave ferrites, etc. The number of papers published in the area of microwave materials and applications has increased considerably over the years, as shown in Figure 1.1.

In 1897, Lord Rayleigh demonstrated that an infinitely long cylindrical rod made up of dielectric material could serve as a waveguide [1]. In 1939 Richtmeyer theoretically predicted that a suitably shaped dielectric piece can function as a microwave resonator [2]. However, it took about 20 years to test Richtmeyer's prediction experimentally. In the early 1960s Okaya and Barash experimented [3, 4] with rutile single crystals and measured the relative permittivity in the microwave frequency range. In 1965 Cohn first reported [5] a dielectric resonator-based device – the filter. A dielectric resonator (DR) is a solid puck, usually ceramic, which can function as a resonator in the microwave and millimeter wave bands. The resonance is similar to that of a circular hollow metallic waveguide except for

Microwave Materials and Applications, First Edition.
Edited by Mailadil T. Sebastian, Rick Ubic and Heli Jantunen.

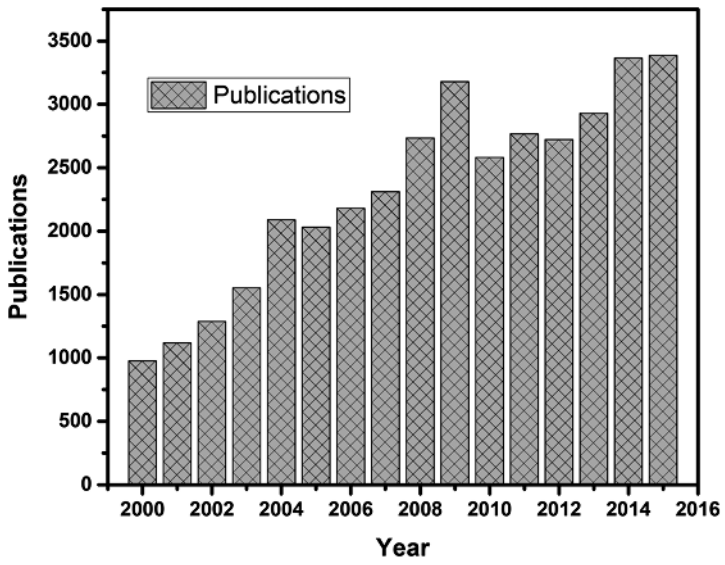

Figure 1.1 *Plot of number of papers published versus year (as per scopus.com using the keyword microwave materials).*

the boundary being defined by a large change in permittivity rather than by a conductor. The resonant frequency is determined by the overall physical dimensions of the resonator and the dielectric constant of the material. As the dielectric constant increases, the resonant frequency decreases. Dielectric resonators are extensively used in the fabrication of oscillators (DRO), bandpass and bandstop filters, dielectric resonator antenna, etc. In the microwave frequency range, the dielectric properties of materials are obtained by analyzing the behavior of electromagnetic waves that pass in the dielectric resonator (DR). Traditionally DRs are made from ceramic materials with high permittivity and high Q factor or low dielectric loss in the microwave region. These DRs are usually prepared in appropriated form by the solid-state ceramic route. They are much smaller in size compared to their metallic counterparts. The three important characteristics of an ideal DR are high relative permittivity (ε_r) for resonator applications and low ε_r for millimeter wave and substrate applications, low dielectric loss (loss tangent), and low coefficient of temperature variation of the resonant frequency (τ_f). The dielectric properties of different types of microwave materials such as DRs, HTCC/LTCC sheets, polymer–ceramic laminates, EMI shielding materials, microwave ferrites, etc., are measured by different techniques depending on their geometric shape, size, and properties [6, 7]. The present chapter elaborates the different techniques used for measuring the microwave dielectric properties.

1.2 Permittivity (ε_r) and quality factor (Q)

The relative permittivity (ε_r) is the physical property of a material that is associated with its energy storing capacity when a potential is applied across it. It is related to the macroscopic properties like polarization or capacitance. The miniaturization process of some devices or

circuits is usually made easier by employing a high ε_r material. A high ε_r facilitates circuit miniaturization because the wavelength inside the DR is inversely proportional to the square root of its permittivity, as given by

$$\lambda_d = \frac{\lambda_0}{\sqrt{\varepsilon_r}} \tag{1.1}$$

where

λ_d = wavelength in the dielectric
λ_0 = wavelength in air (actually in vacuum)
ε_r = real dielectric permittivity

The dimension of the dielectric sample must be an integral multiple of half-wavelength in the dielectric to resonate in the simplest fundamental mode [8]. If that wavelength is reduced, then the physical dimensions of the resonator must be reduced as well. The permittivity of a material determines the relative speed that an electrical signal can travel in it. A low permittivity will result in a high signal propagation speed. When microwaves enter a dielectric material, they are slowed down by a factor roughly equal to the square root of the permittivity, which implies that the wavelength decreases by the same amount and the frequency is unaffected, as shown in Figure 1.2.

The signal propagation is one of the most important aspects in electronic packaging. This is a direct function of the relative permittivity. In the case of ceramic packages, the relative permittivity of the ceramic over and within the metal lines is deposited or embedded governs the propagation delay, t_d, which is given by [9]

$$t_d = \frac{l\sqrt{\varepsilon_r}}{c} \tag{1.2}$$

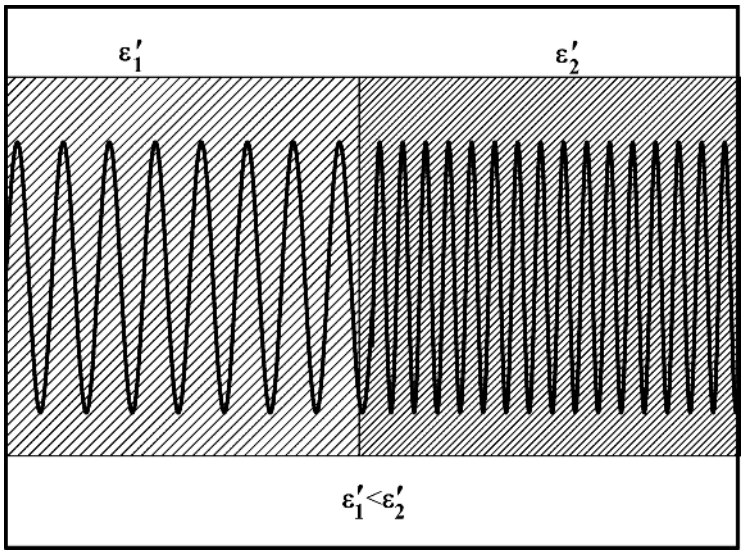

Figure 1.2 *The wavelength is reduced by a factor of $\sqrt{\varepsilon}$ when the wave enters the dielectric.*

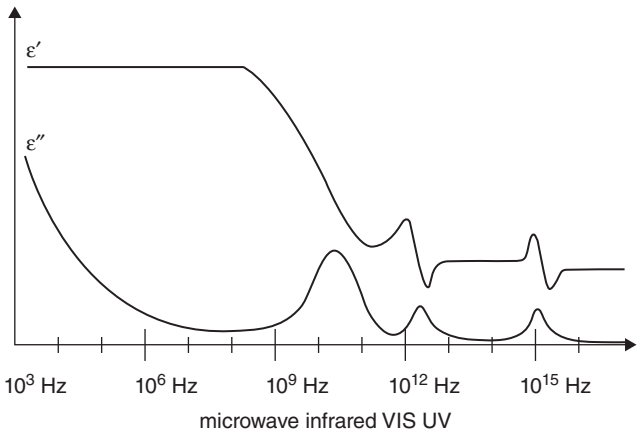

Figure 1.3 *Frequency dependence of polarization processes and peak power losses.*

where l is the line length, ε_r is the relative permittivity of the substrate, and c is the speed of light. Thus substrates with low relative permittivity are required to increase the speed of the signal [10].

By definition, the ε_r is related to the refractive index n ($\varepsilon_r = n^2$). The dielectric permittivity is frequency dependent, and it is very rare that the square of the refractive index measured at optical frequencies is the same as permittivity measured at microwaves. In some materials following this rule, like diamond (ε_r = 5.68, n^2= 5.85) or germanium (ε_r = 16, n^2= 16.73) [11], the same polarization processes are excited by both optical and microwave (or RF) frequencies. In other materials, this rule is not valid since dipolar polarization processes that occur at lower frequencies do not usually occur at higher optical frequencies, that is, the polarization processes are not the same in both frequency ranges. In the microwave frequency region, ionic and electronic polarization mechanisms contribute predominantly to the net dipole moments and the permittivity as depicted in Figure 1.3.

The dielectric loss tangent (tan δ) of a material is associated with dissipation of the electrical energy due to different physical processes such as electrical conduction, dielectric relaxation, dielectric resonance, and loss from non-linear processes [12, 13]. Another concept of dielectric loss is explained by the delay between the electric field and the electric displacement vectors [14]. The dielectric loss of the material is the total sum of intrinsic and extrinsic losses presented by a material. Gurevich and Tagantsev developed a complete theory of intrinsic dielectric losses and these dielectric losses are the losses in the perfect crystals that depend on the crystal structure and can be described by the interaction of the phonon system with the AC electric field [15, 16]. The equilibrium of the phonon system is changed when an AC electric field is applied and a relaxation is observed that is associated with energy dissipation [15, 17]. The dielectric relaxation occurs at low frequency and the phonon frequency is much higher than the microwave frequency. Hence the heat dissipation observed in this relaxation in the ideal lattice should be of anharmonic origin. The dielectric losses are related to the crystal symmetry, AC field frequency, and temperature (intrinsic

features) and these intrinsic losses fix the lower limit of losses in defect-free single crystals or ideal pure materials.

The imperfections in the crystal lattice such as impurities, microstructural defects, grain boundaries, porosity, microcracks, order–disorder, random crystallite orientation, dislocations, vacancies, dopant atoms, etc. (extrinsic features), can also lead to losses. These extrinsic losses can be, in principle, minimized by proper material processing. The losses due to different types of defect show different frequency and temperature dependence. The crystals belonging to different symmetry groups have very different temperature and frequency dependences of dielectric loss [15].

In the microwave frequency range, dielectric ceramics often use the term "quality factor" for the reciprocal of tan δ. The quality factor, or Q, is a measure of the power loss of a microwave system that is defined as

$$Q = 2\pi \frac{\text{Maximum energy stored per cycle}}{\text{Average energy dissipated per cycle}} \tag{1.3}$$

Some losses for a microwave resonator are described as: (a) dielectric, (b) conduction, (c) radiation, (d) external [8]. The dielectric Q_d, conduction Q_c, and radiation Q_r quality factors and these losses are given by

$$Q_d = 2\pi \frac{W_1}{P_d T} = \frac{\omega_0 W_1}{P_d}, \quad Q_c = \frac{\omega_0 W_1}{P_c}, \quad Q_r = \frac{\omega_0 W_1}{P_r}$$

where W_1 is the total stored electric energy in the resonator, ω_0 is the angular resonant frequency, P_d, P_c, and P_r represent the power dissipated in the dielectric, conductor, and radiation, respectively, and

$$T = \frac{2\pi}{\omega_0}$$

The unloaded quality factor Q_u is related as the sum of the other Q-factors by the relation

$$\frac{1}{Q_u} = \frac{1}{Q_d} + \frac{1}{Q_c} + \frac{1}{Q_r} \tag{1.4}$$

where $1/Q_d$ is dielectric loss, $1/Q_c$ is the loss due to conductivity of the metallic plates, and $1/Q_r$ is the loss due to radiation. The radiation loss can be ignored in most resonant cavities because these are completely shielded and so there is no radiation effect.

External losses ($1/Q_{ext}$) arise due to coupling between the resonator and feed. To introduce an electromagnetic field in the resonator, microwave conducting probes are brought close to it (few millimeters of separation) – the higher the ε_r of the resonator, the closer the probe must be to it. The electromagnetic fields around them induce electromagnetic fields in the dielectric ceramic, and so they are coupled. However, the presence of conducting probes in the electromagnetic field lines of the resonator leads to additional loss. The total or loaded Q-factor is defined as [8]

$$\frac{1}{Q_L} = \frac{1}{Q_d} + \frac{1}{Q_c} + \frac{1}{Q_r} + \frac{1}{Q_{ext}} \tag{1.5}$$

where $1/Q_L$ is the total loss of the system and $1/Q_{ext}$ is the loss due to external coupling.

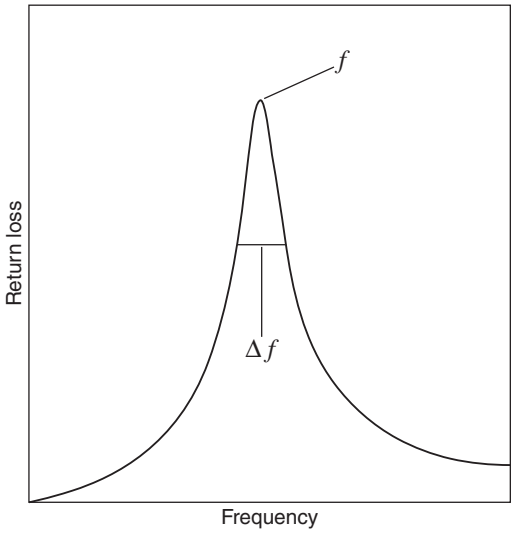

Figure 1.4 *The $TE_{01\delta}$ resonant peak and associated parameters.*

Q_L is determined experimentally from the shape of the resonance peak, as illustrated in Figure 1.4. A bandwidth (BW) is defined as the width of the resonance curve at half power points (3 dB down from the peak). The peak frequency (resonant frequency) f divided by the 3 dB width is equal to Q_L.

The loaded Q_L is obtained from the measured resonant frequency f and half power (–3 dB) bandwidth Δf of TE_{011} mode resonance:

$$Q_L = \frac{f}{\Delta f} \tag{1.6}$$

In practice, resonators are often used with adjustable couplings that allow such approximation without the need for measuring coupling coefficients. If conduction, radiation, and external losses are negligible, then $Q_L = 1/\tan\delta$. When we measure the dielectric loss, at a particular frequency, we get the total loss tangent and we cannot distinguish the contributing factors.

If all conduction, radiation, and external losses are negligible, then the loaded Q-factor depends on dielectric losses in the resonant structure. If the resonant structure contains several (N) dielectrics (one of them is the sample under test) then the Q-factor due to dielectric losses is related to the dielectric losses in particular dielectric regions by the following formula [14]:

$$\frac{1}{Q_d} = \sum_{i=1}^{N} P_{ei} \tan\delta_i \tag{1.7}$$

where P_{ei} is the electric energy filling factor for the ith dielectric region and is defined by

$$P_{ei} = \frac{\iiint_{vd} \varepsilon_i |E|^2 \mathrm{d}v}{\iiint_{vt} \varepsilon\,(v)\,|E|^2 \mathrm{d}v} \tag{1.8}$$

where V_d is the volume of the dielectric resonator, v_t is the volume of the whole resonant structure, $\varepsilon(v)$ is the spatially dependent permittivity inside the whole resonant structure, and ε_i is the permittivity of the ith dielectric region.

In most practical structures conductor losses appear and this must be accounted for in order to determine the Q-factor due to dielectric losses (Q_d) from measured values of the loaded Q-factors:

$$\frac{1}{Q_c} = \frac{R_s}{G} \tag{1.9}$$

The geometric factor G is defined as [14]

$$G = \omega \frac{\iiint_{vi} \mu_0 |H|^2 \mathrm{d}v}{\iint_S |H_t|^2 \mathrm{d}s} \tag{1.10}$$

where μ_0 is the permeability of the resonator.

The coupling losses ($1/Q_{ext}$) are usually determined experimentally and are given by

$$\frac{1}{Q_u} = \frac{1}{Q_d} + \frac{1}{Q_c} + \frac{1}{Q_r} = \frac{1/Q_L}{1 + \beta c_1 + \beta c_2} \tag{1.11}$$

where βc_1 and βc_2 are coupling coefficients for a resonator with two coupling ports. The radiation loss is negligible when the sample is kept in a closed cavity.

1.3 Measurement of Microwave Dielectric Properties

The knowledge of dielectric properties in a different frequency range is important for characterizing the dielectric materials for different practical applications. The precise measurement of the dielectric properties is essential for predicting the device performance. Several methods have been developed and employed for measuring permittivity and permeability of materials in the high-frequency region. The resonant cavity method has been used as the most accurate measurement technique. However, this method has the disadvantage that the measured results are applicable only over a narrow frequency band. Electrical properties of material over a wide range of frequencies can be measured with less accuracy using the transmission line methods. The transmission and reflection methods are used to evaluate the dielectric properties of medium- and high-loss materials as a function of frequency [14, 18].

There are various methods that enable measurement of the quality factors of low-loss dielectrics [18–25], but none of them consider the practical effects like noise, crosstalk, coupling losses, transmission line delay, and impedance mismatch. Inadequate accounting of these effects may lead to significant uncertainty in the measured Q-factor. Determination of the complex permittivity and other electromagnetic properties require precise measurements of the resonant frequencies and Q-factors. For some measurement techniques, these parameters have to be measured in the presence and absence of the test sample, but for other techniques only once in the presence of the test sample is needed. Once the resonant frequencies, Q-factors of the resonant structures, and dimensions of the test samples are measured, computations have to be performed to obtain ε_r and $\tan\delta$.

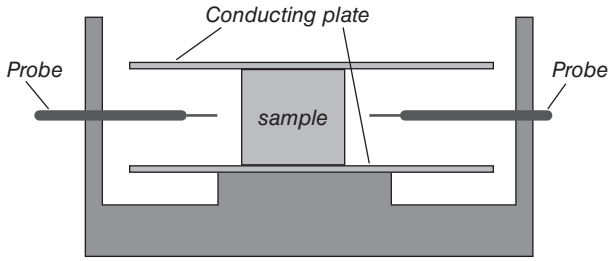

Figure 1.5 *Schematic sketch of the Courtney setup for measuring the dielectric constant under an end shorted condition.*

1.4 Methods of Measurement

1.4.1 Hakki and Coleman (Courtney) Method

1.4.1.1 Permittivity

The complex permittivity of the material of the dielectric resonator is often measured using the method developed by Hakki and Coleman [19] and modified by Courtney [20] in which a cylindrical resonator of material is inserted between two mathematically infinite conducting plates, as shown in Figure 1.5. The end plates are usually made of well-polished copper plates coated with silver or gold. Consider the cylindrical resonator with relative permittivity ε_r, length L, and diameter D placed between the end metal plates (see Figure 1.5). The diameter of the conducting plates should be much larger than that of the dielectric puck. The dielectric properties are obtained by TE_{011} mode analysis. The dielectric puck diameter to height ratio should be about 2 to get wide mode separation, so that the TE_{011} mode is not disturbed by other adjacent modes. If the dielectric material is isotropic then the characteristic equation for such a resonant structure for the TE_{0ml} mode is [19] given by

$$\alpha \frac{J_0(\alpha)}{J_1(\alpha)} = -\beta \frac{K_0(\beta)}{K_1(\beta)} \tag{1.12}$$

where $J_0(\alpha)$ and $J_1(\alpha)$ are the Bessel functions of first kind of order zero and one, respectively. $K_0(\beta)$ and $K_1(\beta)$ are the modified Bessel functions of second kind of orders zero and one, respectively. The parameters α and β depend on the geometry, the resonant wavelength inside the dielectric resonator, and dielectric properties. Thus

$$\alpha = \frac{\pi D}{\lambda_0}\left[\varepsilon_r - \left(\frac{l\lambda_0}{2L}\right)^2\right]^{1/2} \tag{1.13}$$

$$\beta = \frac{\pi D}{\lambda_0}\left[\left(\frac{l\lambda_0}{2L}\right)^2 - 1\right]^{1/2} \tag{1.14}$$

where

l = longitudinal variations of the field along the axis
L = length of the DR
D = diameter of the DR
λ_0 = free space resonant wavelength

The real part of the permittivity of the resonator can be calculated using the mode chart parameters (α_1 and β_1), the resonant frequency (f), and the dimensions of the dielectric puck using the equation

$$\varepsilon_r = 1 + \left[\frac{c}{\pi D f}\right]^2 \left(\alpha_1^2 + \beta_1^2\right) \tag{1.15}$$

Hakki and Coleman [19] used an iris coupling from a waveguide to couple a microwave to the DR. Later Courtney [20] modified the method by using two horizontally oriented E-field probes for coupling the microwave to the dielectric resonator. This enabled a wide range of frequencies to be spanned, since there is no cut-off frequency for coaxial lines. The TE_{011} mode is used for the measurements since this mode propagates inside the sample but is evanescent outside the dielectric resonator sample. Therefore a large amount of electrical energy can be stored in high Q dielectric resonators [25]. In the end shorted condition the E field becomes zero close to the metal wall and electric energy vanishes in the air gap [21]. The TE and TM modes do not contain electric and magnetic fields in the axial (z) direction. The TE_{011} mode is chosen for measurement because for this mode only azimuthal component of the electric field exists and the error due to the air gap is practically eliminated [26]. For a cylindrical resonator, TE and TM modes exist only if the azimuthal mode index $m = 0$; otherwise all other modes are hybrid; that is, they have all six electromagnetic components. Hybrid modes are usually divided into two mode families: HE and EH. They are only occasionally used in measurements of dielectrics (uniaxially anisotropic crystals).

Figure 1.6 shows the frequency response of the TE_{011} mode resonator. By knowing the diameter D and length L of the sample, β is calculated using Equation (1.14). The permittivity ε_r is calculated using Equation (1.15). To avoid the error due to surface roughness the sample should be well polished. In this method, the accuracy is limited by precision of the measurement of the resonant frequency and the dimensions of the sample. The possible error in the measurement of permittivity is of the order of 0.3%. Such an error is possible when dimensional uncertainties of the samples are of the order of 0.15%. The simple measurement setup is the advantage of this method. This is one of the fairly accurate and the most frequently used techniques for measurement of permittivity and this method is proposed as one of the international standards IEC techniques [27] for measurements of the complex permittivity of low-loss solids. In the Courtney method, the ε_r is measured only at one resonant frequency corresponding to the TE_{011} mode. By identifying other resonant TE modes such as TE_{021}, TE_{031}, TE_{041}, etc., it is possible to measure ε_r in a range of frequencies. The quasi-TM modes and TM modes are not suitable for ε_r measurements due to the fact that a minute air gap between the dielectric sample and the metal plate considerably alters the resonant frequency, which affects the accuracy of ε_r measurement [23, 28].

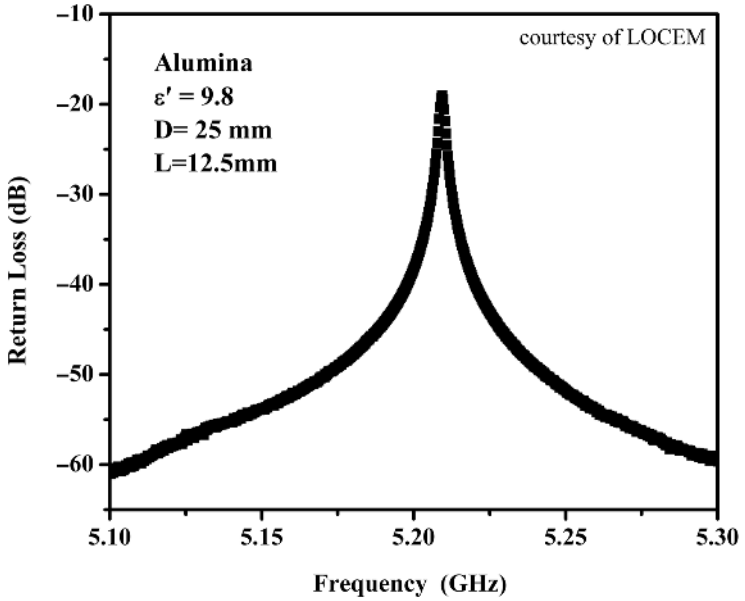

Figure 1.6 *The TE_{011} resonance of a ceramic puck with ε_r = 9.8 under an end shorted condition.*

1.4.1.2 Measurement of Loss Tangent

The quality factor for the TE_{011} mode can be measured using the Hakki and Coleman method [18–21, 23, 29–31]. The quality factor measured by this method will be low since loss occurs due to the conducting plates and radiation effects. However, correction to conductor losses can be applied knowing the surface resistance of the conducting plates. The unloaded Q_u is obtained from the measured resonant frequency f and half power (–3 dB) bandwidth Δf of TE_{011} mode resonance given by (1.6).

The tan δ can be calculated [18–21, 23, 29–31] from

$$\tan\delta = \frac{A}{Q_u} - BR_s \quad = A\left[\frac{1}{Q_u} - \frac{R_s}{A/B}\right] = \frac{1}{P_e}\left[\frac{1}{Q_u} - \frac{1}{Q_c}\right]$$
$$A = 1 + \frac{W}{\varepsilon_r}; B = \left(\frac{\lambda_0}{\lambda_g}\right)^3 \left(\frac{1+W}{30\pi^2\varepsilon_r l}\right); W = \frac{{J_1}^2(\alpha)}{{K_1}^2(\beta)} \frac{K_0(\beta)K_2(\beta) - {K_1}^2(\beta)}{{J_1}^2(\beta) - J_0(\alpha)J_2(\alpha)} \tag{1.16}$$

where Q_c is given by Equation (1.9) and $G = A/B$ and $P_e = 1/A$. R_s is the surface resistance of the conducting plates and is given by [29]

$$R_s = \sqrt{\frac{\pi f \mu}{\sigma}} \tag{1.17}$$

where

σ = conductivity of the conducting plates
μ = permeability for a non-magnetic metal = $4\pi \times 10^{-7}$ H/m

λ_0 = resonant wavelength
$\lambda_g = 2L/l$ ($l = 1, 2, 3,\ldots$)
λ_g = guiding wavelength of an infinitely long dielectric rod wave guide
W = ratio of electric field energy stored outside to inside the rod [22, 29]

Kobayashi and Tamura [29] has reported a method of measuring the value of R_s using two rod samples cut from a dielectric rod that have the same diameters but different lengths. One of the rods for a TE_{01p} mode resonator is p times as long as the other for a TE_{011} mode resonator where $p \geq 2$. The modes have almost the same resonant frequency but differ in observed unloaded quality factors because of different conductor loss contributions in the two cases. Since both rods have the same tan δ, the following equation can be obtained:

$$R_s = 30\pi^2[\lambda_g/\lambda_0]^3 \frac{\varepsilon_r + W}{1 + W} \frac{p}{p-1} \left[\frac{1}{Q_{ml}} - \frac{1}{Q_{mp}}\right] \tag{1.18}$$

where Q_{ml} and Q_{mp} are measured unloaded quality factors for TE_{011} and TE_{01p} modes, respectively.

1.4.2 $TE_{01\delta}$ Mode Dielectric Resonator Method

The Q-factor of a dielectric resonator sample measured by the Hakki–Coleman or Courtney method can be affected by the conductor and radiation losses. These effects can be avoided by using the cavity method in which the DR is kept on a low-loss single crystal quartz or Teflon spacer inside the cavity. The quality factor (Q), permittivity (ε_r), and τ_f of the DRs can be measured using a transmission mode cavity proposed by Krupka *et al.* [14, 32]. Figure 1.7 shows the cavity setup for the measurement of the Q-factor.

The DR is placed inside a cylindrical metallic cavity usually made of copper and the inner surfaces are finely polished and usually gold or silver coated and the cavity is closed after loading the DR sample. The cavity is fed using loop coupling. The cavity has an infinite number of modes when excited with a microwave spectrum of frequencies. Usually a D/L ratio of about 2 is maintained to get maximum mode separation and to avoid interference from other adjacent modes. For high-permittivity materials, the first mode is the $TE_{01\delta}$

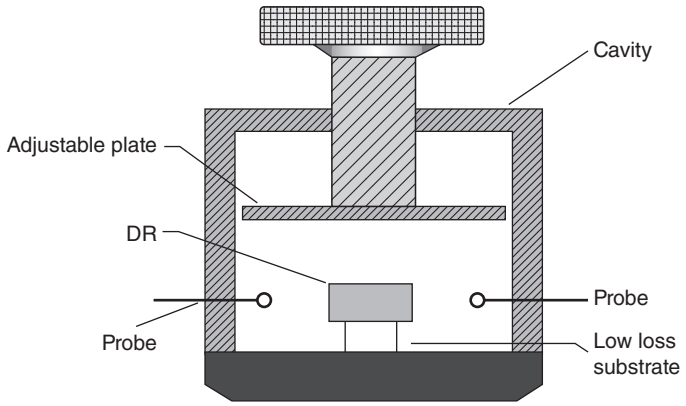

Figure 1.7 *The cavity setup for the measurement of Q-factor.*

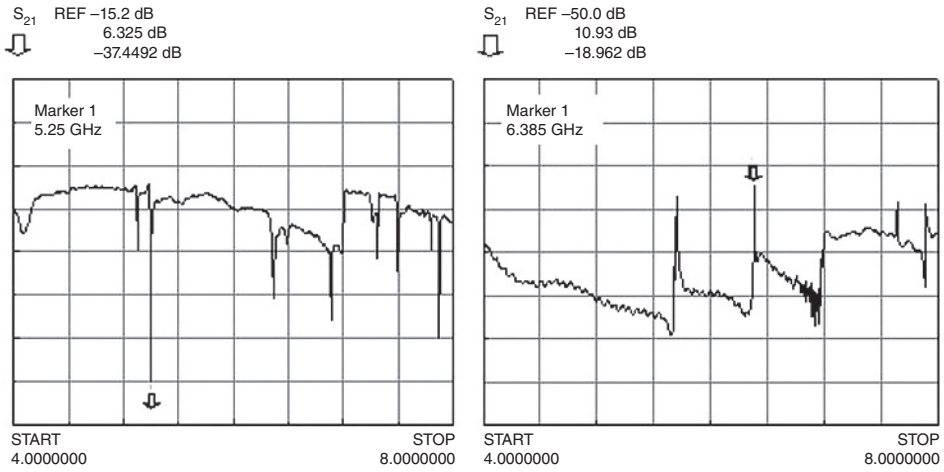

Figure 1.8 *Microwave resonance spectra of $Ba(Mg_{1/3}Ta_{2/3})O_3$ ceramic with $\varepsilon_r = 24$: (a) reflection and (b) transmission configuration.*

mode but for low-permittivity materials a few modes may appear before the $TE_{01\delta}$ mode. The resonant frequency, quality factor, and τ_f are dependent on the resonator surroundings.

The electric field is symmetric with the geometry of the sample and the cavity, which helps to reduce the sources of loss due to cavity. In the $TE_{01\delta}$ cavity method, the field confinement is not complete in the z direction and hence the TE_{011} mode is designated as $TE_{01\delta}$. As seen in Figure 1.7, the sample is isolated using low-loss substrate (a quartz or a Teflon spacer), from the effects of losses due to the finite resistivity of the metallic cavity. Figure 1.8 shows the typical resonance spectra of $Ba(Mg_{1/3}Ta_{2/3})O_3$ ceramic ($\varepsilon_r = 24$). One can assume that the unloaded Q-factor is equal to the loaded Q-factor if the coupling is weak. The $TE_{01\delta}$ mode frequency is noted and the unloaded Q-factor is measured.

After identifying the mode, the resonant frequency and 3 dB bandwidth are determined. From this, the coupling coefficient βc_1 and βc_2 for the coupling ports are determined using the relations $\beta c_1 = (1 - S_{11})/(S_{11} + S_{22})$ and $\beta c_2 = (1 - S_{22})/(S_{11} + S_{22})$, where S_{11} and S_{22} are reflection coefficients of port 1 and port 2 in magnitude [33].

From the measured Q_L, Q_u can be calculated using Equation (1.11). Sometimes, the desired mode (the $TE_{01\delta}$ one) may be close to other modes. In such cases the cavity volume can be slightly changed by rotating the top screw, which moves the top plate up or down that separates the modes. The ability to tune the frequency is very useful for the identification of the desired resonant mode and to allow it to measure samples of various dimensions. Figure 1.9 shows a typical test fixture manufactured by QWED. Rigorous electromagnetic analysis must be performed to evaluate permittivity and the dielectric loss tangent of the sample under test. The Rayleigh–Ritz method has been used in a computer program for a typical test fixture manufactured by QWED.

The $TE_{01\delta}$ mode method is one of the most accurate techniques for measuring loss tangent and permittivity of isotropic low-loss materials [32, 34]. Assuming that all parasitic losses can be neglected (that are small for $TE_{01\delta}$ mode if permittivity of the sample is large)

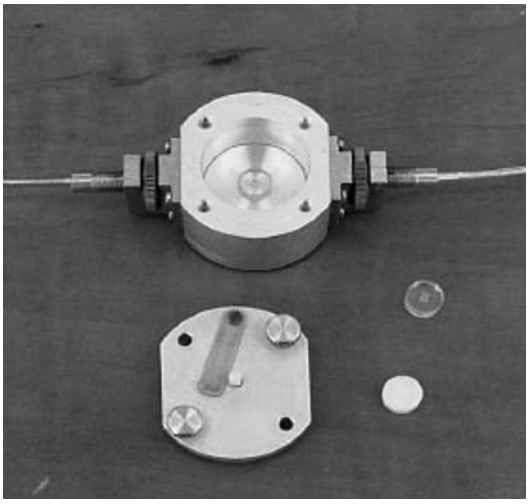

Figure 1.9 *The cavity manufactured by QWED for the quality factor measurement.*

and assuming that the electric energy filling factor is equal to unity, the inverse of the measured unloaded Q-factor is approximately equal to the dielectric loss tangent. Moreover, these assumptions are not valid for very low-loss dielectric materials (in this case conductor losses must be rigorously taken into account) and for low-permittivity materials (the electric energy filling factor in the sample is substantially smaller than 1).

The cavity method using the $TE_{01\delta}$ mode has several advantages, such as easy mode identification, small parasitic losses, and lack of mode degeneracy [14]. However, the evaluation of ε_r and tan δ requires advanced numerical computations (this can only be done by employing dedicated computer programs) because of the absence of exact solutions of Maxwell's equation. For this reason the Hakki and Coleman method is still used as it allows relatively easy determination of permittivity.

The uncertainty in dielectric loss tangent using the $TE_{01\delta}$ mode cavity method with optimized enclosure is of the order of $\pm\, 2 \times 10^{-6}$ or 0.03 tan δ (whichever is larger) and uncertainty of ε_r measurements is $\Delta\varepsilon/\varepsilon = \pm\, \Delta$ dim/dim (where dim = dimensions of the test sample). The measurement frequency depends on the size and permittivity of the test samples. Measurements at higher frequencies are possible by using smaller cavities and smaller test samples or by using several higher order quasi-TE_{0nm} modes [35].

The presence of resonator support and the coupling loop can perturb the electromagnetic field and this may lower the Q value and shift the resonant frequency [36]. In order to minimize this perturbation caused by the support and coupling loop, the test cavity should be large. However, on increasing the size of the test cavity, the resonant modes of the cavity move to lower frequencies. When ε_r of the dielectric resonator is larger than about 20, the $TE_{01\delta}$ mode of the dielectric resonator shifts to below the first test cavity mode (TM_{010}). Valant *et al.* observed that the electromagnetic field could penetrate into the conducting walls of the test cavity (skin effect) lowering the measured Q value of the dielectric resonator [36]. The test cavity size should be large in order to avoid the skin

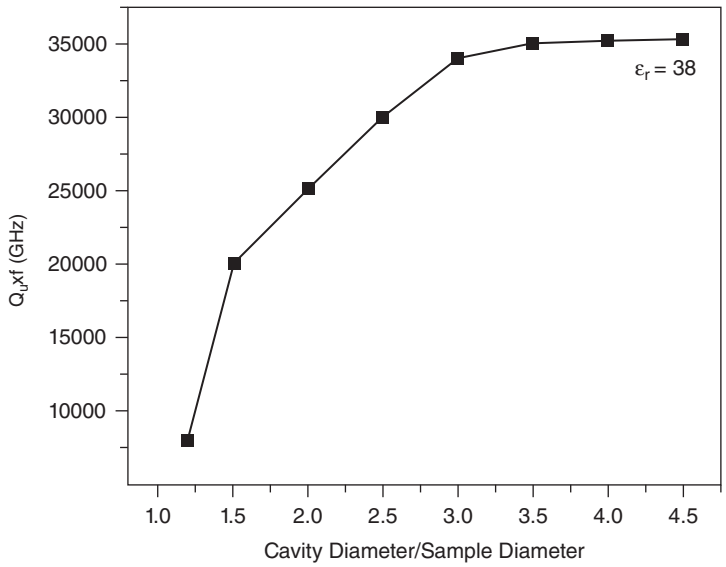

Figure 1.10 *Variation of Qf with ratio of the cavity diameter/sample diameter.*

effect. The quality factor decreases when the cavity diameter/puck diameter ratio is smaller than 3, as shown in Figure 1.10.

Normally, the size of cavity used is 3–5 times of the test sample. The contribution of the surface resistance of metals of the cavity can be calculated from the quality factor of the TE_{011} resonance of the empty cavity before calculating losses by conduction of the cavity walls. This value can be applied to correct the measured Q of the sample [8]. One can measure ε_r and tan δ at low frequencies by the parallel plate capacitor method using an LCR meter for new materials. This will give an approximate idea of ε_r and tan δ and in turn will help to calculate the approximate resonant frequency of the DR using the following equation [37]:

$$f \propto \frac{1}{v_r\sqrt{\varepsilon_r}} \tag{1.19}$$

where v_r is the volume of the DR.

Knowledge of the value of the resonant frequency will further help to find the size of the DR at a given frequency or the size of the cavity required to measure the Q-factor.

1.4.3 Measurement of the Quality Factor by a Strip Line Excited Using the Cavity Method

In the microstrip line excited cavity method, the dielectric resonator is magnetically coupled to a 50 ohm microstrip line, as shown in Figure 1.11, along with the equivalent circuit [38].

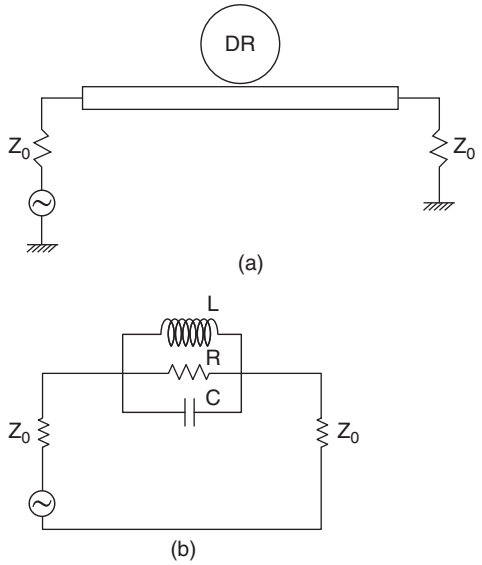

Figure 1.11 *Schematic diagram of a DR coupled to (a) a microstrip line and (b) an equivalent circuit. (After Khanna and Garault [38]).*

The ratio of the resonator coupled resistance R at the resonant frequency to the resistance external to the resonator is called the coupling factor β_c:

$$\beta_c = \frac{R}{R_{ext}} = \frac{S_{110}}{S_{210}} \tag{1.20}$$

where S_{110} and S_{210} are the real quantities representing the reflection and transmission coefficients, respectively, at the resonant frequency.

Under critical coupling ($\beta_c = 1$), the power dissipated in the external circuit is equal to the power dissipated in the resonator (P_d), which is equally divided into the power reflected to the generator ($P_r = {S_{110}}^2$) and the power transmitted to the load ($P_t = {S_{210}}^2$). In the shielded resonator configuration, from the conservation of energy, power dissipated in the resonator is given by

$$P_d = 1 - |S_{110}|^2 - |S_{210}|^2 \tag{1.21}$$

The coupling factor β_c is a function of the distance between the dielectric resonator and the microstrip line under fixed shielding conditions. The expression for the unloaded voltage transmission coefficient S_{21u} derived by Khanna and Garault is given by [38]

$$S_{21u} = S_{210}\sqrt{\frac{2}{\left(1 + {S_{210}}^2\right)}} \tag{1.22}$$

where S_{21u} corresponds to the voltage transmission coefficient of the unloaded resonator.

The frequencies f_1 and f_2 corresponding to S_{21u} given by Equation (1.22) is obtained from the network analyser (Figure 1.12). The difference in frequencies ($f_2 - f_1$) is Δf. The

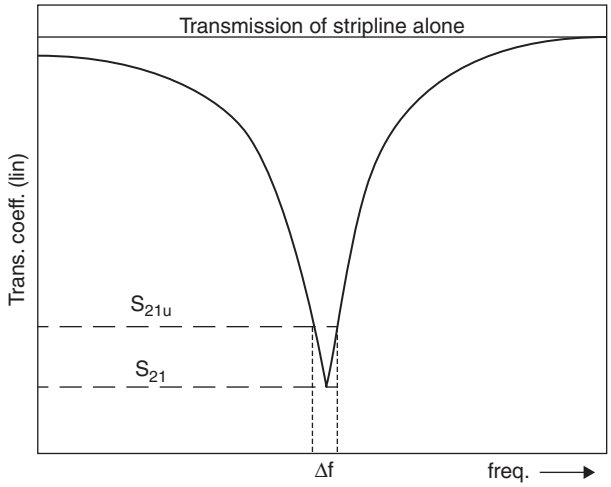

Figure 1.12 *Typical resonant curve of a DR coupled to a microstrip line used in determining the quality factor by the strip line method.*

frequency corresponds to the peak of the S_{21} curve is the resonant frequency. Knowing the resonant frequency f and Δf, the unloaded quality factor, Q_u, is calculated using Equation (1.6).

Figure 1.13 shows the experimental setup for the Q measurement by the microstrip line excited cavity method. A 50 Ω microstrip line of width 3 mm is etched on RT-Duroid 5880 ($\varepsilon_r \sim 2.2$ and thickness 1.9 mm) and kept at the bottom wall of a rectangular cavity made of copper. The cavity is excited using 3.5 mm microstrip edge connectors as shown in Figure 1.13. The dielectric resonator is placed near the microstrip line and the resonance spectra is observed on the network analyzer.

The $TE_{01\delta}$ mode is identified from among the different modes. Set the central frequency as the resonant frequency and reduce the span to enhance the frequency resolution. Then the network analyzer is calibrated for S_{21} THRU by connecting an identical microstrip

Figure 1.13 *The experimental setup for measuring the quality factor by the strip line method. The DR is coupled to the strip line.*

transmission line used in the cavity. Then connect it to the cavity with DR and measure the resonant frequency *f*. The transmission coefficient S_{210} corresponding to *f* is taken. The factor S_{21u} is calculated using Equation (1.22). From the width Δf corresponding to S_{21u} and *f*, the unloaded quality factor is calculated.

1.4.4 Whispering Gallery Mode (WGM) Resonators

The $TE_{01\delta}$, $TM_{01\delta}$, or $HE_{11\delta}$ modes are the main modes used in dielectric measurements by the Courtney, $TE_{01\delta}$, or strip line methods [19, 20, 30, 34] and the *Q* measured by these methods depends on dielectric loss of the material as well as on the radiation and conductor losses of the cavity. Hence a simple measurement of the quality factor by the Courtney, $TE_{01\delta}$, or microstrip line methods is not sufficient to determine accurately the dielectric loss of low-loss dielectric materials.

It was reported [39–45] that Whispering Gallery modes (WGMs) would confine the entire fields within the resonator, which in turn give negligible radiation and conductor losses at microwave frequencies. The quality factor of the WGM dielectric resonator is limited only by the intrinsic losses in the dielectric material. The measured WGM Q-factor is approximately equal to 1/tan δ.

In WGM resonators, most of the electromagnetic energy is confined to the dielectric near the perimeter of the air–dielectric interface, which in turn reduces the radiation and conductor losses [41, 43]. The WGM technique allows measurements of two permittivity components of uniaxially anisotropic materials (several single crystals exhibit uniaxial anisotropy). Permittivity components can be determined from measurements of resonant frequencies and Q-factors of two modes belonging to different mode families employing rigorous numerical analysis, for example, mode-matching. The electrical energy filling factors for E (quasi-TM mode) and H (quasi-TE mode) modes are given by [41, 44, 45]

$$P_{\varepsilon_\perp} = 2\frac{\partial f}{\partial \varepsilon_\perp}\frac{\varepsilon_\perp}{f}; \quad P_{\varepsilon||} = 2\frac{\partial f}{\partial \varepsilon_{||}}\frac{\varepsilon_{||}}{f} \tag{1.23}$$

The dielectric loss tangent for the dielectric can be solved [43, 44] using the equation:

$$Q_E^{-1} = \tan\delta(P_{\varepsilon\perp} + P_{\varepsilon||}) + R_s/G_E \tag{1.24}$$

$$Q_H^{-1} = \tan\delta(P_{\varepsilon\perp} + P_{\varepsilon||}) + R_s/G_H \tag{1.25}$$

where

R_s = surface resistance of the cavity enclosing the DR
εll = permittivity parallel to the anisotropic axis
$\varepsilon_\perp$ = permittivity perpendicular to it

The conductor losses decrease as the surface resistance becomes smaller and as the geometric factor (*G*) increases [45]. The geometric factor *G* is significantly large and the effect of losses due to cavity walls can be ignored when compared to the loss tangent. The energy filling factors (WGM modes) of DR for all these modes are close to unity and will have high quality factors. In effect, acting on these modes, radiation losses are negligible. The WGM method offers good suppression of spurious modes because the propagation constant along the *z* axis is very small and unwanted modes leak out axially. The WGM modes offer a high level of integration. The WGM dielectric resonators are classified as either $WGE_{n,m,l}$

in which the electric field is essentially transverse or $WGH_{n,m,l}$, for which the electric field is essentially axial. The integer n denotes the azimuthal variation, m radial variation, and l the axial ones. WGMs are periodic according to the azimuthal number, and the number of modes in a bandwidth increases with the diameter of the DR. Therefore, for a small diameter of the resonator, the frequency interval between two successive modes will be large. Dielectric resonators acting on their WGMs can be excited in different ways. In the low-frequency range, one can use an electric or magnetic dipole. However, this type of excitation is stationary and traveling WGM cannot be excited. In the millimeter wave region either dielectric image waveguides or microstrip transmission lines are used to excite traveling WGMs.

1.4.5 Split Post Dielectric Resonator (SPDR)

The split post dielectric resonator (SPDR) provides an accurate method for measuring the complex permittivity and loss tangent of substrates and thin films at a single frequency point. The sample should be in the form of a flat rectangular piece or a sheet [46–50]. The SPDR uses a particular resonant mode, which has a specific resonant frequency depending on the dimensions and the dielectric constant of this resonator. This method does not have flexibility in the measurement of frequency and dimensions as the samples need to be prepared in the form of thin sheets. In this method, flat samples of the test material are inserted through one of the open sides of the fixture. The laminar dielectric under test is placed between two low-loss dielectric rods or resonators kept in a metallic enclosure, as shown schematically in Figure 1.14. The sample must be very thin with parallel faces. The air gap between the sample and the dielectric resonator does not affect the accuracy of the measurement. The required thickness of the sample also depends on the ε_r of the material. Materials with high ε_r must have less thickness.

The setup for the SPDR method consists of a pair of dielectric resonators and a metal enclosure of relatively small height. This configuration allows formation of an evanescent electromagnetic field, not only in the air gap between the dielectric resonators but also in the

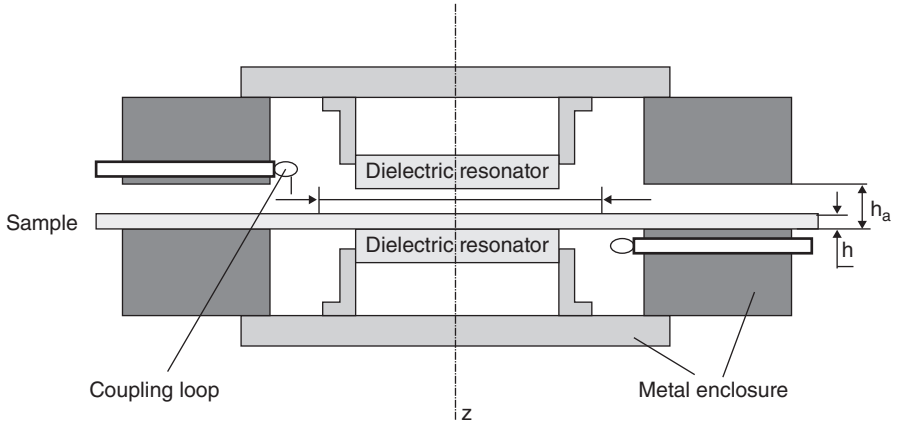

Figure 1.14 *Schematic sketch of SPDR.*

cavity region for radii greater than the radius of the dielectric resonator. This simplifies the numerical analysis and reduces possible radiation effects. Although different modes of the resonator can be identified and used for the microwave characterization, the $TE_{01\delta}$ mode is preferable since this mode is insensitive to the presence of air gaps perpendicular to the z axis of the fixture. The thickness of the sample needs to be measured and is provided as a parameter to evaluate the dielectric properties.

The complex permittivity can be calculated based on the rigorous electromagnetic modeling of the split post resonant structure using the Rayleigh–Ritz technique [47]. The real part of the complex permittivity can be computed from the measured resonant frequencies and thickness of the sample using the following equation [47]:

$$\varepsilon_r' = 1 + \frac{f_0 - f_s}{h f_0 K_\varepsilon \left(\varepsilon_r', h\right)} \tag{1.26}$$

where h is the thickness of the test sample, f_0 is the resonant frequency of the empty SPDR, f_s is the resonant frequency of the SPDR with the dielectric sample, and K_ε is a function of ε_r' and h has to be evaluated for a number of ε_r and h using the Rayleigh–Ritz technique [47]. The iterative procedure is used to evaluate subsequent values of ε_r' from Equation (1.26). The loss tangent of the test sample is calculated from the measured unloaded Q-factors of the SPDR with and without the dielectric sample based on

$$\tan\delta = \left(\frac{1}{Q_u} - \frac{1}{Q_{DR}} - \frac{1}{Q_c}\right)/P_e \tag{1.27}$$

where Q_{DR}^{-1} and Q_c^{-1} denote losses of the metallic and dielectric parts of the resonator, respectively, and P_e is the electric energy filling factor of the sample given by Equation (1.8). Uncertainty of the dielectric measurements of a sample of thickness h can be estimated as $\Delta\varepsilon/\varepsilon = \pm\,(0.0015 + \Delta h/h)$ and $\Delta \tan\delta = 2 \times 10^{-5}$ or $\pm\, 0.03 \tan\delta$ for dielectric permittivity and uncertainty in loss tangent measurements, respectively.

The dielectric properties measured by SPDR methods are obtained for only one frequency determined by dimensions and dielectric permittivity of the resonator. Thus each SPDR is designed for a particular nominal frequency and the actual measurement is taken close to the nominal frequency; this determines the requirements for the size of the sample. For example, for SPDR of nominal frequency 5–6 GHz, the minimum sample size should be 30 × 30 mm and thickness 2.1 mm. QWED manufactures SPDRs with dedicated software for the evaluation of permittivity and loss tangents. SPDR has superior accuracy as compared to the reflection-transmission methods. The method is convenient and quick to measure low-loss laminar dielectrics such as substrates or LTCC, printed circuit boards, and even thin films and is not suitable for dielectric resonators. Classically, the most precise measurements with resonators have been performed employing network analyzers. Recently QWED developed an **inexpensive computer-controlled microwave oscillator system** (microwave frequency Q meter), which enables quick and automatic measurements with a dedicated SPDR [48]. Figure 1.15 shows the general view of a microwave frequency Q meter connected to the SPDR and to the computer manufactured by QWED. The hardware part of the Q meter consists of the PLL-stabilized microwave source with DDS generated reference controlled by a fast 32-bit ARM microcontroller. A wideband logarithmic

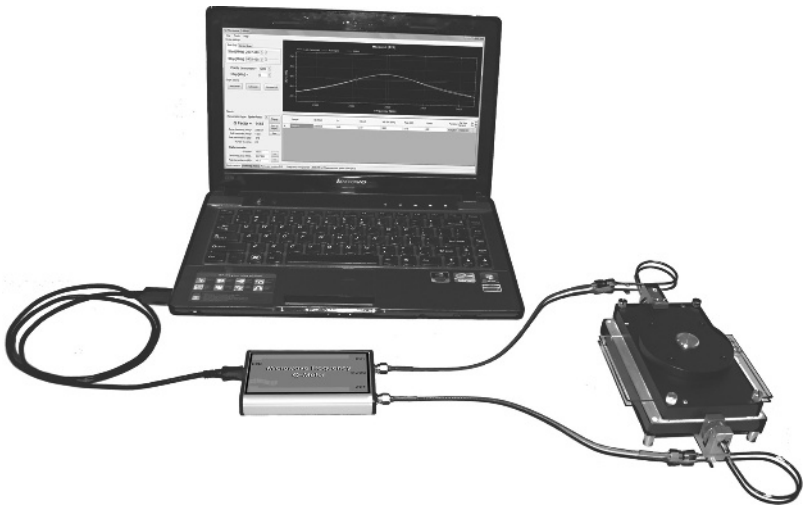

Figure 1.15 *Photographs of SPDR connected to a Q meter and computer. Source: Reproduced with permission from QWED, Poland.*

power detector is used to measure the transmitted power level through the resonator. A multipoint resonance curve-fitting algorithm enables the Q-factor to be accurately calculated. The only external information required is the thickness of the sample under test. The good hardware simplicity as well as the use of a computer screen for presentation of the results leads to a significant cost reduction to start exploration of electromagnetic properties of materials with SPDR. The microwave frequency Q meter can be connected to the computer via a USB port. The relative permittivity and dielectric loss tangent can be easily measured with dedicated SPDRs. These Q meters are available in the frequency range up to 5.2 GHz (type: 4.4 GHz ÷ 5.2 GHz; type II: 1.4 GHz ÷ 2.6 GHz; type II: 0.7 GHz ÷ 1.3 GHz).

1.4.6 Cavity Perturbation Method

The cavity perturbation technique was a method used to obtain approximate solutions but its applications were limited not only to low-permittivity samples but also to specific modes and specific samples. The cavity perturbation technique is widely used for the determination of the dielectric characteristics of thin sheet samples of low and medium dielectric loss [18, 51]. In the cavity perturbation technique, a small piece of the material, usually in the form of a disk or sheet, is placed in a metallic resonant cavity operating in a known mode. The material characteristics are estimated from the shift in the resonant frequency and change in the Q of the system [52–55].

This technique was developed by Slater [55] and is used to measure the dielectric properties of materials with permittivity less than 10. The cavity perturbation method provided frequencies determined by cavity and DR dimensions and hence it is not a swept frequency measurement. The cavity is excited with optimum iris coupling; typically the diameter of the iris is equal to the shorter dimension of the waveguide (WG)/2.2 and can be used for the measurement of dielectric properties of the samples.

The resonant frequency and quality factor of the empty cavity is determined for different cavity modes. After measuring frequency and quality factor the thin sheet sample is inserted and positioned at the E-field antinode. If the sample is purely dielectric the maximum electric field can be easily determined by simply moving the sample across the slit. The mode will shift to the low frequency side and retraces from there. The sample is kept at the retracing position where the electric field is maximum. If the sample is slightly magnetic the permittivity can be measured only for the odd modes by keeping it at the middle of the cavity. The new resonant frequency and Q of the sample is again measured. The complex dielectric constant of the sample is calculated [18, 51, 56] using the following equations:

$$\varepsilon_r' = 1 + \left[\frac{V_c(f_0 - f_s)}{2V_s f_s}\right] \tag{1.28}$$

$$\varepsilon_r'' = \frac{(\varepsilon' - 1)}{2\varepsilon'} \frac{f_s}{(f_0 - f_s)} \left[\frac{1}{Q_s} - \frac{1}{Q_0}\right] \tag{1.29}$$

$$\tan\delta = \frac{\varepsilon_r''}{\varepsilon_r'} \tag{1.30}$$

where

f_0 = resonant frequency of the empty cavity
f_s = resonant frequency of the cavity with sample
V_c = volume of the cavity
V_s = volume of the sample
Q_0 = quality factor of the empty cavity
Q_s = quality factor of the cavity with sample

The experimental error is found to be less than 2% in the case of permittivity and 1.3% in the case of dielectric loss. Here also the measured Q_s and Q_0 can be corrected by measuring S_{11} and S_{22}, as mentioned earlier, by proper calibration of the network analyser. The main advantage of this method is the easiness of determining the permittivity and loss using a simple device with moderate accuracy.

1.4.7 TM_{0n0} Mode and Re-entrant Cavity Methods

The microwave dielectric properties can also be measured in the frequency range 2–10 GHz using the TM_{0n0} mode cavities with rod dielectric samples [57, 58]. In the frequency range 50 MHz to 2 GHz a re-entrant cavity method can be employed [59, 60] to evaluate the dielectric properties. Both TM_{010} and re-entrant cavities are closed with a lid after insertion of the samples. For the TM_{010} mode cavity, a transcendental equation is known only if the height of the sample is equal to the height of the cavity. For a re-entrant cavity, the exact solution for a transcendental equation in a closed form does not exist. It can be solved using rigorous mode-matching methods [60]. Karpova [61] was the first to present a mode-matching numerical technique to solve Maxwell's equation for a re-entrant cavity. Since the electric energy filling factor in the re-entrant cavity is close to unity, resolution in the loss tangent measurement is of the order of 5×10^{-5}. A similar resolution in the loss tangent is possible for the TM_{010} mode cavities provided the test sample has a sufficiently large diameter. The uncertainty in a real permittivity measurement is about 0.5–2% for the TM_{010}

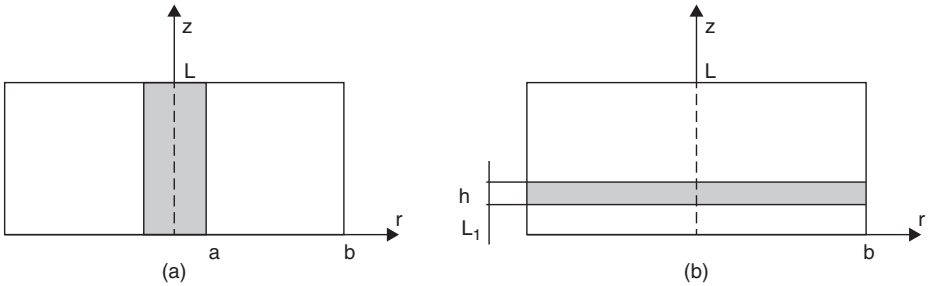

Figure 1.16 *Cylindrical cavities containing (a) a dielectric rod and (b) a dielectric disk.*

mode cavity and about 1–3% for the re-entrant cavity. The loss tangent and permittivity can be measured as a function of frequency by employing higher-order TM_{0n0} modes.

1.4.8 TE_{01n} Mode Cavities

Complex permittivity and Q-factor of low-loss disk samples (Figure 1.16) can be measured by the TE_{01n} mode method [62–64]. Normally, the operating frequency range for these cavities is in the range 8–40 GHz. The TE_{01n} mode in the cavities have a circumferential electric field distribution, which is tangential to a cylindrical sample kept symmetrically in the cavity [14]. Hence, the electric field is continuous across dielectric–air interfaces that allow an air gap omission without degradation of measurement uncertainties. The physical contact between the lateral surface and the cavity bottoms is not important since the surface currents in the metal cavity walls are circumferential.

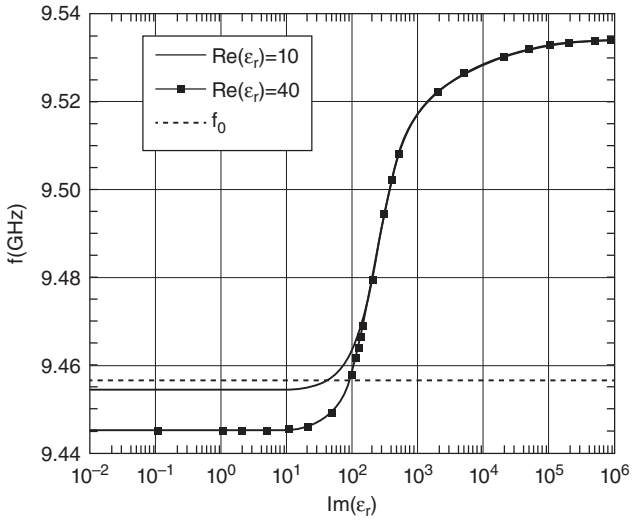

Figure 1.17 *Variation of resonant frequency with an imaginary part of permittivity for the TE_{011} mode cylindrical cavity with a dielectric disk sample. Dotted line corresponds to the TE_{011} mode frequency of the empty cavity. Source: Adapted from Krupka 2006 [14].*

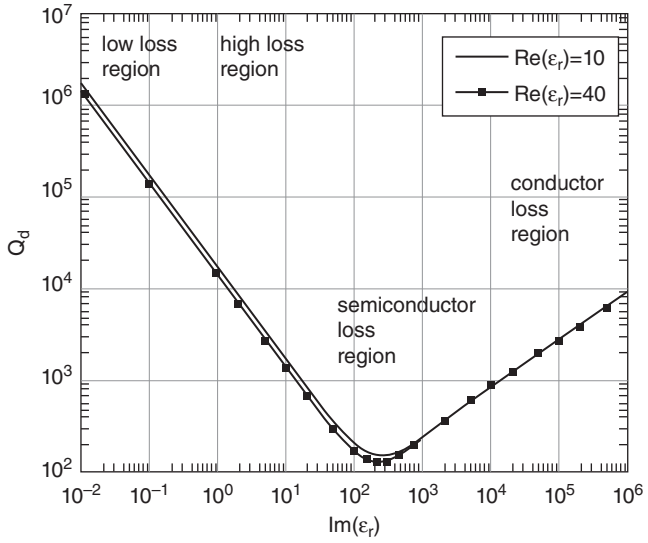

Figure 1.18 *Variation of Q-factor due to dielectric losses as a function of the imaginary part of permittivity for the TE_{011} mode cylindrical cavity containing a dielectric disk sample. Source: Adapted from Krupka 2006 [14].*

The variations of resonant frequency and Q-factor due to dielectric losses versus the imaginary part of permittivity for the TE_{011} mode cylindrical cavity containing the dielectric sample are shown in Figures 1.17 and 1.18. The resonant frequency is smaller than that for the empty cavity (Figure 1.17) in the low-loss dielectric region. The resonance frequency displacement ($f_0 - f$) depends on the real permittivity and thickness of the sample. The quality factor due to dielectric loss in this region is given by Equation (1.9) and depends linearly on the dielectric loss tangent.

The real part of the complex permittivity can be determined from the measured resonant frequency and the simplified transcendental equation in the low dielectric loss region, where both complex permittivity and complex angular frequency have imaginary parts equal to zero. The surface resistance in a closed cavity can be determined from the measured Q-factor of the empty cavity and then scaling up to the frequency of the cavity containing the sample using the formula

$$R_s(\omega) = R_s(\omega_0)\sqrt{\frac{\omega}{\omega_0}} \tag{1.31}$$

where ω_0 is the resonant angular frequency of the empty cavity.

When the imaginary part of permittivity becomes very large (see Figure 1.18), then both the resonant frequency and the Q_d depend on the imaginary part of the permittivity. In this case only the imaginary part of permittivity can be determined. For low-loss materials the TE_{01n} mode cavities method can be employed using thicker samples. The ideal thickness of the sample is a half wavelength or its multiple [14]. The electric energy filling factors in the dielectric sample become relatively large and a higher resolution loss tangent measurement

(5×10^{-5}) can be achieved. The uncertainty in the permittivity measured using TE_{01n} mode cavities is of the order of 0.5% [14]. At lower frequencies, < 8 GHz, the dimensions of the TE_{01n} mode cavities and samples become too large for practical applications.

1.4.9 Thin Samples and Free-Space Methods

The microwave dielectric properties of thin samples can be measured using the Kent [49] method, the Yu–Cullen [65] method, and the free-space method [18, 66–68]. The size of the sample should be larger than the wavelength of the electromagnetic wave. To further minimize the effects of the scatterings from the sample boundary, the sample size should be twice larger than the wavelength. The wave that is incident in the sample must be planar, for this condition the separation between antenna and sample (d) must fulfill the relation

$$d > \frac{2D^2}{\lambda}$$

where λ is the wavelength of the operating electromagnetic wave and D is the largest dimension of the antenna aperture. The measurement results may be affected by the environment [69]. At lower frequencies, the effects of the environment are more serious. To minimize these effects, it is recommended to conduct free-space measurements in an anechoic chamber. Meanwhile, one can also use time-domain gating to eliminate the unwanted signal caused by environment reflections and multireflections.

1.4.9.1 Free-Space Methods

Free-space techniques for the study of magneto-dielectric material properties measurements have several advantages. In the traditional techniques, some problems associated with interfaces (materials/air/hollow metallic waveguides), such as the inhomogeneity of dielectric material, contactless, and air gaps, can promote unwanted higher-order modes excited in the measurements, but this problem does not exist in free-space measurement.

Free-space measurements are realized by reflection methods like short-circuited reflection (Figure 1.19) and metal-backing and bistatic reflection (Figure 1.20). The basis of these methods is measuring the reflection caused by a metal plate kept close to the sample and the interference caused in this reflection due to the dielectric properties of the sample.

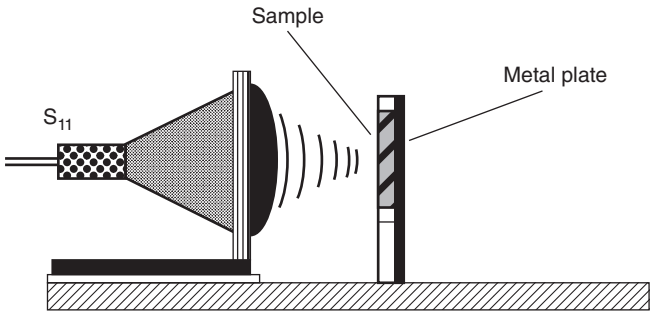

Figure 1.19 *Setup for free-space by the short-circuited reflection method.*

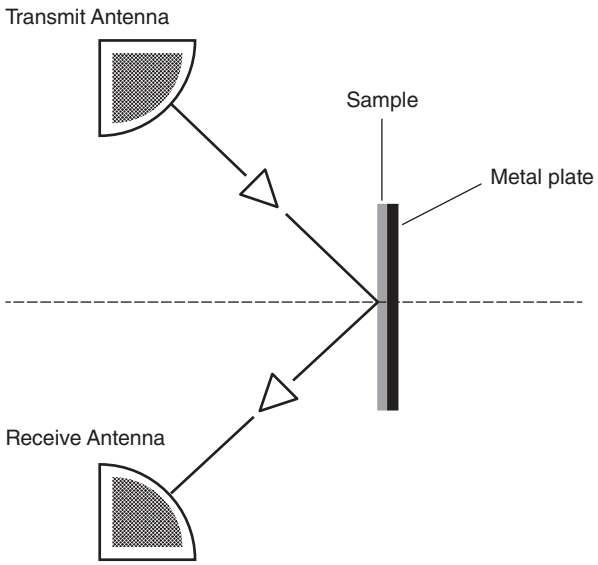

Figure 1.20 *Setup for free-space by metal-backing and bistatic reflection.*

The measurement of permittivity is given by

$$S_{11} = \frac{jz\tan(\beta d) - 1}{jz\tan(\beta d) + 1}; \quad z = \frac{1}{\sqrt{\varepsilon_r}}; \quad \beta = \frac{2\pi}{\lambda}\sqrt{\varepsilon_r} \tag{1.32}$$

where z is the wave impedance of material normalized to the wave impedance of free space and β is the phase constant of the material. However, the permittivity of the sample cannot be expressed explicitly in terms of S_{11} and d, and numerical methods are often used in the calculation of dielectric permittivity.

It is possible to make accurate free-space measurements at microwave frequencies by using precision horn lens antennas that have far-field focusing ability. The typical measurement setup consists of two antennas and a sample holder as shown in Figure 1.21. The

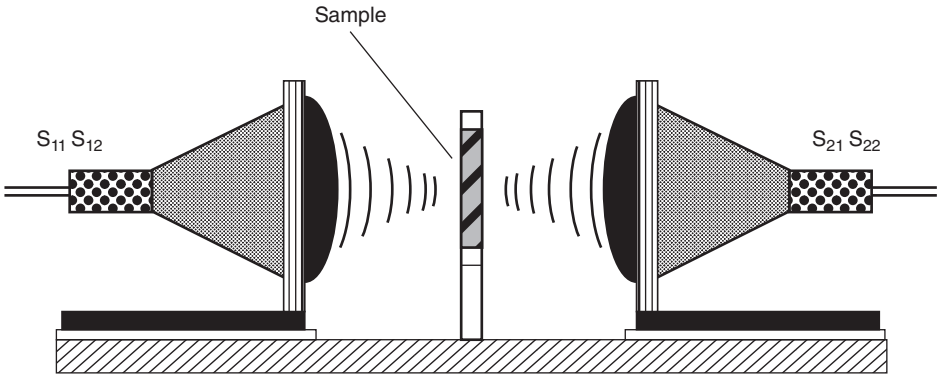

Figure 1.21 *Accurate setup for free-space measurements.*

transmission and reception antennas are spot-focusing horn lens antennas. The effects of sample boundaries and the measurement environment are minimized by using focusing antennas. A specially fabricated sample holder is placed at the common focal plane for holding planar samples. The microwave signal incident to planar samples can be taken as plane waves, and the properties of the sample under test are obtained from the reflection and transmission through the sample. The dielectric and magnetic properties are obtained by relations of S parameters obtained by reflection and transmission of horn lens antennas in a free-space setup:

$$S_{11} = \frac{\Gamma(1 - T^2)}{1 - \Gamma^2 T^2}$$
$$\varepsilon_r = \frac{\gamma}{\gamma_0}\left(\frac{1 - \Gamma}{1 + \Gamma}\right)$$
$$S_{21} = \frac{T(1 - \Gamma^2)}{1 - \Gamma^2 T^2}$$
$$\mu_r = \frac{\gamma}{\gamma_0}\left(\frac{1 + \Gamma}{1 - \Gamma}\right)$$

where

S_{11} and S_{21} are S parameters for reflection and transmission, respectively
T and Γ reflection coefficients and transmission, respectively
μ_r = relative permeability
ε_r = relative permittivity
γ and γ_0 are propagation constant of the sample and of free space, respectively

The free-space measurements are commonly accompanied by a precise mathematic algorithm; the Nicolson–Ross–Weir (NRW) algorithm, for example, is very much utilized in the measurements of free space.

1.4.9.2 Sheet Resonator or Kent method

The dielectric properties of microwave substrates can be measured by the method proposed by Kent [49]. The sheet sample is kept between the flat flanges of the two metal circular waveguides as shown in Figure 1.22. The dielectric properties of the sheet can be calculated from the resonant frequency and the quality factor of the TE modes excited in the waveguide. The transmission through the sheet sample of the TE mode reaches its maximum at a frequency below the cut-off frequency of the waveguides and above the cut-off frequency of the cylindrical portion of the sample. The frequency of these TE modes can be obtained from the waveguide radius, thickness, and the dielectric constant of the sheet sample.

For the TE_{01} mode, the reciprocal of the unloaded quality factor is given by

$$\frac{1}{Q_0} = \frac{(\varepsilon_r''/\varepsilon_r') + (\delta/a)(\theta_c/\theta_0)^2 U}{1 + U} \tag{1.33}$$

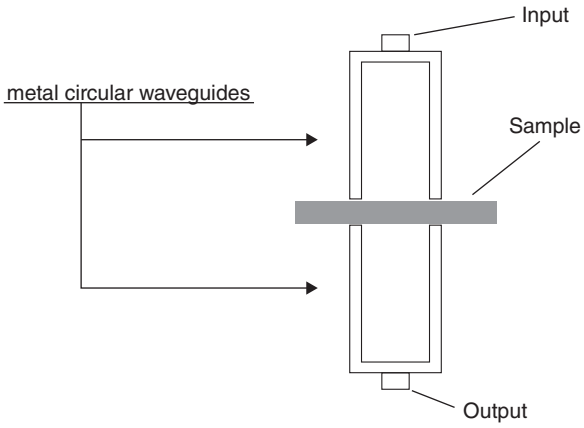

Figure 1.22 *Schematic for dielectric measurement by the Kent method.*

where δ is the skin depth of the waveguide wall, $(\varepsilon_r' - j\varepsilon_r'')$ is the relative complex permittivity of the substrate, a is radius of waveguide and [49]

$$\varepsilon_r' U = \frac{\cos^3\theta}{(\theta + \sin\theta\cos\theta)\sin\theta} \tag{1.34}$$

where the quantity U is the ratio of the electric energy in the waveguide to that in the substrate. The value of U increases when the resonant frequency f_0 approaches the cut-off frequency f_c and the dielectric constant ε_r' decreases.

1.4.9.3 Open Resonator Method (Yu–Cullen Method)

The use of the cavity resonator can be difficult in the microwave frequency range. This is due to the fact that the resonator size is directly proportional to the wavelength and the quality factor of a cavity resonator varies with the wavelength as $\lambda^{3/2}$. The decrease is rather rapid as the wavelength decreases. Hence, at high microwave frequencies the measurements in cavity resonators can be difficult [70].

This difficulty can be overcome by using the open resonators [71]. The important feature of an open resonator is that the number of modes is proportional to the length rather than the volume of the resonator. This method usually works in the frequency range of 10 to 200 GHz. Using the open resonator method, flat disk-shaped solid samples can be measured, and liquids or powders can be measured provided they are restrained within a solid annulus, which is outside the microwave beam area and covered by plates with a low dielectric constant and a low loss tangent.

Yu–Cullen [65] used a biconcave open resonator and the measurement configuration is shown in Figure 1.23. A parallel plane-sided slab of dielectric material with thickness t is placed midway between two identical spherical mirrors with radius R_0. The total length of the resonator is $L = 2d$ and the distance between the sample plane and the spherical mirror is d. There are two techniques for the measurement of materials properties. In one technique, the length of the cavity is fixed and the resonant frequency is measured with and without the sample. In the other technique, the length of the cavity is adjusted to establish resonance

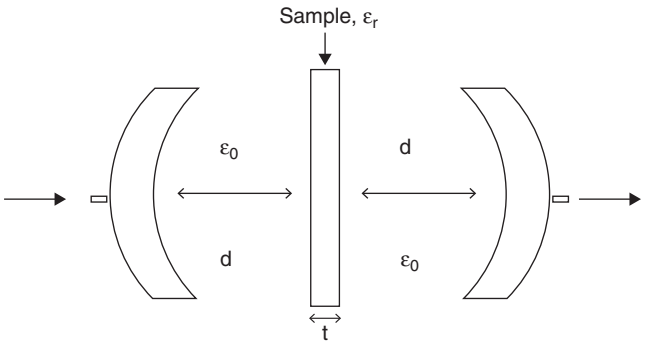

Figure 1.23 *Schematic for dielectric measurement by the Yu–Cullen method.*

with and without the sample at the same frequency. Here, we discuss the basic algorithms for these two techniques, and more detailed discussions can be found in references [65] and [70]. It should be noted that in an open resonator method for materials property characterization, usually the refractive index n is used. For a dielectric material, the relationship between the refractive index and dielectric permittivity is given by

$$n = \sqrt{\varepsilon_r'} \tag{1.35}$$

The relations for measurements of dielectric properties of a sample by the two techniques are shown below. For symmetric modes the variation of frequency is given by

$$\Delta = \frac{n^2}{n^2 \sin^2(nkt - \Phi_T) + \cos^2(nkt - \Phi_T)} \tag{1.36}$$

For assymetric modes:

$$\Delta = \frac{n^2}{n^2 \cos^2(nkt - \Phi_T) + \sin^2(nkt - \Phi_T)} \tag{1.37}$$

For the second technique the solution is

$$d + t = d_0 - p + \frac{t(n - \Delta)}{n^2 k^2 w_t^2} + \frac{3}{4k^2 R_0} \tag{1.38}$$

The rest of the calculation follows along the same lines as the frequency-variation method, solving the transcendental equation for n and iterating if necessary.

The dielectric loss is calculated by equations for symmetric and asymmetric modes:

$$\tan\delta = \frac{2nk(d + t\Delta_s)}{Q[2nkt\Delta_s + \Delta_s \sin 2(nkt - \Phi_T)} \tag{1.39}$$

$$\tan\delta = \frac{2nk(d + t\Delta_a)}{Q[2nkt\Delta_a - \Delta_a \sin 2(nkt - \Phi_T)} \tag{1.40}$$

where k is number wave; t is sample thickness; Φ is an angle of the beam with the axis of the resonator.

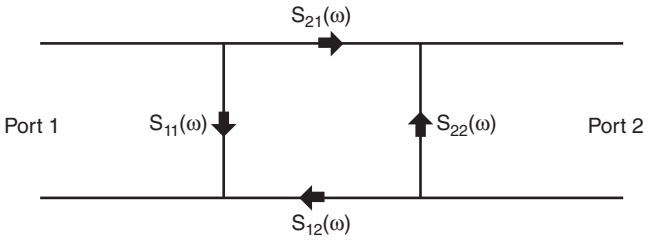

Figure 1.24 *Diagram for the S parameter in the network analyzer.*

1.5 Measurement of EMI Shielding Effectiveness

The EMI shielding measurements are performed by the waveguide method using a vector network analyzer. It is a non-resonant method in which the material under test is inserted into a segment of the transmission line and the properties of the materials are deduced on the basis of the reflection from the material and the transmission through the material.

Since the incident and reflected waves have both magnitude and direction, the *S* parameters are complex numbers. A signal flow graph of a two-port device using *S* parameter notation is shown in Figure 1.24. In the notation $S_{\text{out in}}$, the first number represents the output port and the second number represents the input port.

For a two-port network, the relation between the incident and reflected waves are expressed in terms of $S_{11}(\omega)$, $S_{22}(\omega)$, $S_{12}(\omega)$, and $S_{21}(\omega)$, where $S_{11}(\omega)$ is the response measured at port 1 with the stimulus applied at port 1, $S_{22}(\omega)$ is the response measured at port 2 with the stimulus applied at port 2, $S_{12}(\omega)$ is the response measured at port 1 with the stimulus applied at port 2, and $S_{21}(\omega)$ is the response measured at port 2 with the stimulus applied at port 1. Thus *S* parameters represent the frequency domain response characteristics.

1.5.1 Waveguide Method

In electromagnetic and communication engineering, the waveguide is any linear structure that guides the electromagnetic waves. The dimensions of the waveguide determine the frequency it can support. Waveguide transmission lines are used as a sample holder in this method. The sample is kept inside the wave-guide sample holder coupled to the network analyzer through coaxial waveguide adapters and cables, as shown in Figure 1.25.

In a waveguide, radiated waves undergo reflection, absorption, and transmission. The complex scattering parameters that correspond to the reflection (S_{11} and S_{22}) and transmission (S_{21} and S_{12}) in the samples are measured using the network analyzer. The EMI shielding effectiveness (EMI SE) as well as reflection (SE_R) and absorption (SE_A) shielding effectiveness are calculated from these scattering parameters [72]. If the power fed at port 1 is P_i, power reflected at the same port is P_r, and the output power at port 2 is P_o, then the losses by reflection and absorption is given by the equations

$$SE_R = 10 \log [P_i/(P_i - P_r)] = 10 \log [1/(1 - S_{11})] \tag{1.41}$$

$$SE_A = 10 \log [(P_i - P_r)/P_o] = 10 \log [(1 - S_{11})/(S_{12})] \tag{1.42}$$

$$\text{EMI SE} = SE_R + SE_A \tag{1.43}$$

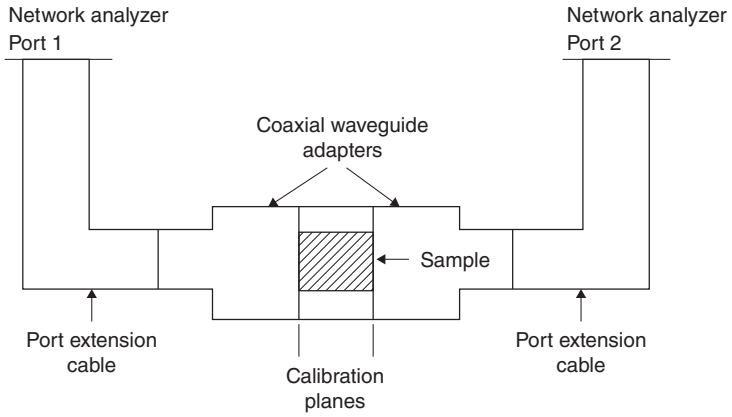

Figure 1.25 *Schematic for the waveguide method.*

Full two-port calibrations were initially done on the test setup in order to remove errors due to directivity, source match, load match, isolation, etc., in both forward and backward directions. The error associated with this measurement is less than 2%. This method has the advantages of easy sample preparation due to the rectangular shape of the sample as well as error due to the air gap can also be avoided. Figure 1.26 shows the measurement setup used in the present example.

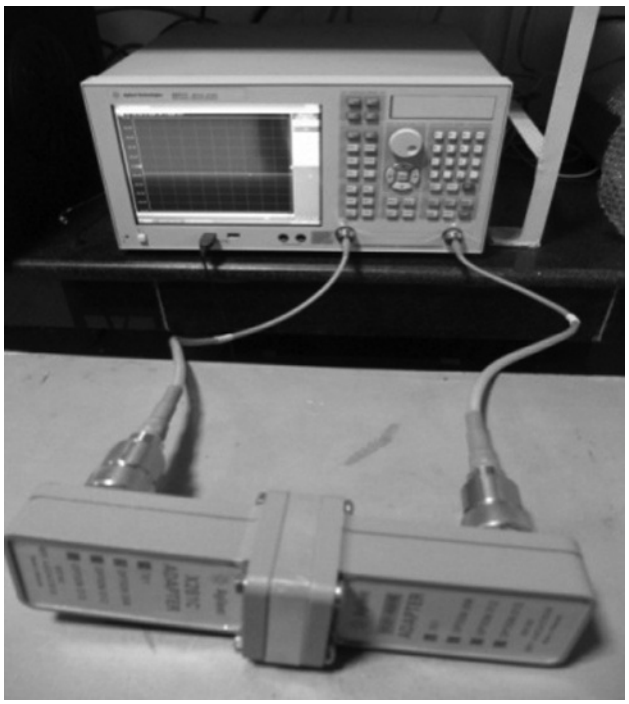

Figure 1.26 *Measurement setup used for cavity methods.*

1.6 Terahertz and Millimeter Wave Measurements

The millimeter wave spectral range is a link between the conventional radio frequency (RF) techniques that work up to approximately 300 MHz. The microwave frequency range (MW) is considered from 300 MHz up to 30 GHz. The millimeter wave range (mm) is considered in between 30 GHz up to 300 GHz. The THz range is generally considered to be 0.3–30 THz. Above 300 MHz stray capacitances and cable length effects lead to errors in the measurement of the components of the electrical impedance, because of the decreasing source intensity and problems associated with finite sample size effects. This frequency is the limit of the THz range. The availability of appropriate sources and detectors, and the development of new experimental measuring configurations lead to the increased importance of the THz range in the study of materials.

1.6.1 Backward Wave Oscillator (BWO)

A backward wave oscillator (BWO), also known as a carcinotron or backward wave tube, is a vacuum tube that is used to generate millimeter waves up to the terahertz range. It is a traveling wave tube. It is an oscillator with a wide electronic tuning range and operates in the range of $\lambda \sim 3$–0.3 mm (100 GHz–1 THz). The study of dielectric and conductive properties of crystals, ceramics, glasses and polymers, powders, composites, liquids, films, and fibers are reported in the literature. The experimental setup for studying the dielectric properties of materials is basically an optical experimental setup measuring channel. In this technique the radiation is normally incident on the sample, which is in the form of a plane-parallel plate. The experiment can either be in a transmission geometry (coefficient T) and phase shift (ϕ) of the transmitted wave or in reflection geometry (coefficient R) and phase shift (ϕ) of the reflection coefficient, which are related to the materials characteristics ε' and ε'' [73]:

$$T = \mathrm{e}^{-4\pi kd/\lambda} \frac{(1-R)^2 + 4R\sin^2\psi}{\left(1 - \mathrm{Re}^{-4\pi kd/\lambda}\right)^2 + 4\mathrm{Re}^{-4\pi kd/\lambda}\sin^2\left(\frac{2\pi\eta d}{\lambda} + \psi\right)} \tag{1.44}$$

$$\phi = \frac{2\pi nd}{\lambda} - \arctan\frac{k(n^2+k^2-1)}{(k^2+n^2)(2+n)n} + \arctan\frac{\mathrm{Re}^{-4\pi kd/\lambda}\sin^2\left(\frac{2\pi nd}{\lambda} + \psi\right)}{1 - \mathrm{Re}^{-4\pi kd/\lambda}\cos^2\left(\frac{2\pi nd}{\lambda} + \psi\right)} \tag{1.45}$$

$$R = \frac{(n-1)^2 + k^2}{(n+1)^2 + k^2}, \psi = \arctan\left(\frac{2k}{n^2+k^2-1}\right), \varepsilon' = n^2 - k^2, \varepsilon'' = 2nk \tag{1.46}$$

where d is the sample thickness, and n and k are the refractive index and extinction coefficients, respectively, that is, the optical parameters of the material. One can use T, ϕR, and ϕ to calculate ε' and ε''.

The quasi-optical BWO spectroscopy is a powerful technique to study the dielectric response of solids in the terahertz to subterahertz ranges. In reality, spectroscopic studies of a variety of materials, ranging from dielectrics to conductors and superconductors, and components like filters and polarizers to food products, are reported in the literature [74–82]. The BWO spectrometers are associated with a wide range of operation (30 GHz to nearly 1.5 THz), high-frequency resolution ($\Delta\nu/\nu \approx 10^{-5}$), and a wide dynamic range

(40–50 dB). The possibility of continuous frequency tuning and the direct measurement of dielectric response spectra are strong characteristics of this technique.

Studies of BWO spectroscopy for biological systems in the millimeter waves and terahertz range are also reported in the literature [83, 84]. In reference [85] a study of tumorous and non-tumorous breast tissues using the backward-wave oscillator-based free-space quasi-optical spectroscopy was employed to obtain transmission data from 30 to 120 GHz. This high-precision experimental technique yields dielectric data with a sensitivity of 10^{-6}, with high accuracy and resolution [86–90]. The results show different characteristics of breast tissues with tumorous and non-tumorous tissues. The technique shows good possibilities for applications for *in vivo* breast cancer detection and diagnostics [85].

1.6.2 Terahertz Time-Domain Spectroscopy (THz-TDS)

The THz range is generally considered to be 0.3–30 THz, where in the literature different definitions can be found. A high interest in this frequency region led to the development of new sources and experimental techniques have been developed to access the THz range [90]. Because of the difficulties in the availability of solid-state THz sources, the research community have focused on all optical techniques producing THz radiation, employing visible/near-IR femtosecond pulsed lasers. This development of broadband THz time-domain spectroscopy (THz-TDS) [91, 92] has led to an increase in the study of the properties of the materials in this region of the spectra. The coherent THz-TDS spectroscopy technique opens the possibility to study the electrical properties of materials, demonstrating the potential use of THz radiation for spectroscopy in a number of application areas. The solid-state THz semiconductor laser and the quantum cascade laser present an active new frontier in the THz area of research [93, 94].

Terahertz time-domain spectroscopy (THz-TDS) is a spectroscopic technique that operates with electromagnetic transients generated using optical femtosecond (1 fs = 10^{-15} s) laser pulses. These THz transients are electromagnetic pulses of duration around 1 ps duration. Their spectral bandwidth varies from frequencies below 100 GHz to 5 THz. The optical detection gives the terahertz electric field with a time resolution of a fraction of a picosecond. From the experimental results the real and imaginary parts of the dielectric function of the material can be obtained. The THz-TDS experimental setup is composed of a femtosecond laser source, a beamsplitter, a THz transmitter, focusing and collimating optics, the sample, a THz detector, and a variable delay line, as shown in Figure 1.27. A computer controls the variable delay line and displays the detector photocurrent versus path length.

The THz switch operates when a laser pulse with photon energy higher than the photoconductor's bandgap energy is focused on the gap of the transmission line. Figure 1.28 shows a photoconductive switch integrated in a microstrip transmission line. In this case, by measuring this signal as a function of the time delay between the arrival of the THz and probe pulses at the electro-optic crystal using a variable delay line, the electric field of the THz pulse in the time domain can be obtained, and the Fourier transform analysis gives the frequency spectrum of the THz radiation pulse. From this measurement, both the real and imaginary parts of the dielectric function of the medium under study may be extracted. The analysis of the transmission and reflection analysis of the THz pulses in thick samples could be done using the measurements of ε' and ε''. In general, broadband THz radiation can be generated either in an optoeletronic manner involving photogenerated transient currents in

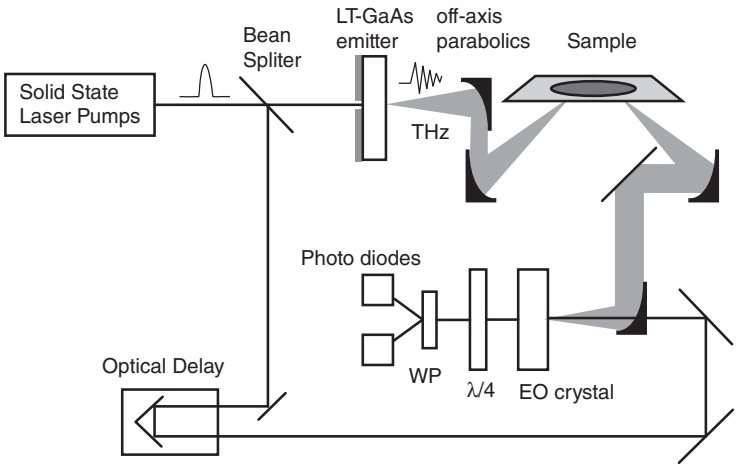

Figure 1.27 *Experimental optical arrangement of a THz system.*

photoconductive antennas [95] or in an optical manner involving optical rectification in EO materials [96].

On the other hand, many groups are looking for new materials such as amorphous electro-optic polymers (EO) that could generate and detect broadband terahertz radiation (0.3−30 THz) [97]. Recently a ∼12 THz, spectral gap-free THz system based on a polymer emitter–sensor pair has been reported in the literature [97]. The THz properties of materials were explored for sensing and identification of explosives, drugs, and controlled materials [98]. Dispersive Fourier transform spectroscopy (DFTS) is another alternative used to study dielectric data of materials in this range of 400 GHz to 1.2 THz [99]. This technique can be used in several interferometer configurations and to study liquids, powders, and gases [99]. In reference [99] the technique was used to study powders of flour, dry milk, corn starch, pesticides, baking soda, and talc.

The refractive index and the real part of the dielectric permittivity were found to be the most reliable for identification and detection purposes. Studies of liquids like ethanol, gasoline, and mixtures are reported in the literature [100], where the frequency-dependent permittivity of mixture solutions provides information concerning the relaxation process in solvent and solute molecules. In this study the dielectric properties of ethanol/gasoline mixtures in the terahertz spectral region are investigated [100]. The relaxation study of both liquids (gasoline and ethanol) are modeled using the Debye model in the THz frequency region.

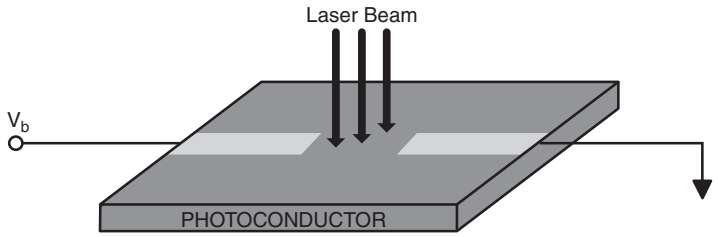

Figure 1.28 *A photoconductive switch integrated in a microstrip transmission line.*

1.7 Measurement of Dielectric Properties of Powder Samples

Dielectric ceramic powders with low loss are extensively used to improve dielectric properties of polymers. In the last 10 years interesting polymer–ceramic composites have been introduced enabling free adjustment of permittivity of devices in several wireless communication applications [101]. In addition, inks based on low-temperature curing polymers with embedded dielectric ceramic particles are used in advanced printed electronics. In these cases it is crucial to know the dielectric properties of powder particles, which can differ significantly as compared to bulk properties. The microwave dielectric properties of powder samples were measured by different techniques [102–108]. Recently Tuhkala *et al.* [106, 109, 110] reported an indirectly coupled open-ended coaxial cavity resonator method operating in TEM mode at 4 GHz to estimate the relative permittivity and loss tangents of powder samples. In this method the open-ended coaxial cavity with optimized dimensions and conductivity is first filled with powder samples. The effective dielectric constant and loss tangent are then determined by the shift in the resonant frequency and change in Q-factor between an empty resonator and a powder sample filled resonator. A schematic setup for the measurement is shown in Figure 1.29.

For a completely filled cavity, the effective dielectric constant is given by

$$\varepsilon_r = {}^{c}\!/_{(4Lf)^2}$$

where c is the speed of the light in vacuum, L is the resonator length, and f is the resonant frequency.

The dielectric constant of powder samples can be obtained from a measured resonator response, volume fractions of each phase (powder, air, and different phases), and calculating the effective dielectric constant using Bruggeman symmetric [111] and Looyenga [112] mixing rules.

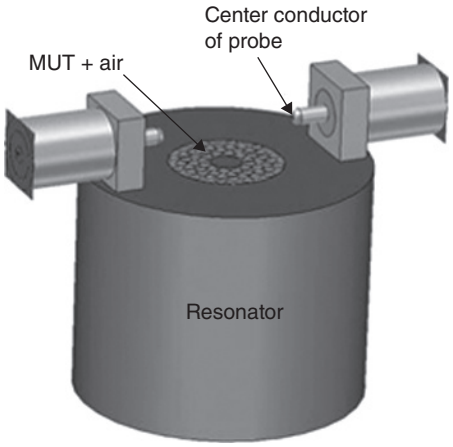

Figure 1.29 *Schematic for dielectric measurements of powder samples. Source: Tuhkala* et al. *2013 [106]. Reproduced with permission of AIP.*

In the same manner the effective loss tangent can be obtained from the following equation, which utilizes general mixing rules:

$$\tan \delta_{eff} = \frac{1}{Q_{filled}} - \frac{1}{Q_{empty}}$$

The method expects careful estimation of the volume fraction of the powder, homogeneous distribution of the powder throughout the cavity, management of the measurement environment (mainly humidity), and probe coupling, which should be loose enough not to disturb the measurement itself and to produce a symmetric resonance peak. Tuhkala *et al.* [109, 110] estimated the microwave dielectric properties of several materials with reasonable accuracy using this technique. They also reported an estimation of the humidity level of the powders [110], the effect of surfactant treatment [113], and an evaluation of the amount of two powder phases [109] using the above method [106].

1.8 Estimation of Dielectric Loss by Spectroscopic Methods

The intrinsic losses in the dielectric material can be obtained by spectroscopic methods using a combination of far-infrared and submillimeter (or THz) spectroscopy [15]. This will give an idea of the lowest possible loss in the sample. It is possible because the intrinsic microwave losses are fully determined by the multiphonon absorption of the ideal (but necessarily anharmonic) crystal and the polar lattice vibration (optic phonons).

The far-infrared reflection spectra can be analyzed by the Kramers–Kronig relation and classical dispersion theory [114–116]. The K-K relationship between r and the phase of reflected wave Θ is given by [114]

$$\begin{aligned} \Theta(\nu) &= \frac{2\nu}{\pi} \int_0^\infty \frac{\ln r(\nu')}{\nu'^2 - \nu^2} \mathrm{d}\nu' \\ r &= \sqrt{R} \\ R(\nu) &= |r(\nu) \quad \exp(i\theta(\nu))|^2 \end{aligned} \tag{1.47}$$

The K-K integration requires data from zero to infinite frequency. The accuracy of the analysis is affected by extrapolation of experimental data taken in the finite frequency range 0 and to infinite frequency. The combination of K-K and classical dispersion theory proves [117] to be a better and more reliable analysis. The optical parameters n and k can be determined from the reflected intensity R and the phase angle Θ using the following relationships [117]:

$$n = \frac{1 - R}{1 + R - 2\sqrt{R}\cos\Theta} \tag{1.48}$$

$$k = \frac{-2\sqrt{2R}\sin\Theta}{1 + R - 2\sqrt{2}R\cos\Theta} \tag{1.49}$$

$$\varepsilon' = n^2 k^2 \tag{1.50}$$

$$\varepsilon'' = 2nk \tag{1.51}$$

where

n = refractive index
ε' and ε'' = real and imaginary parts of the dielectric constant, respectively
K = extinction coefficient

The analysis involves four steps:

(a) The K-K analysis allows the phase angle $\Theta(\nu)$ spectrum to be calculated from the experimental reflectivity spectrum $R(\nu)$.
(b) Calculation of real and imaginary parts of the complex index of refraction using Equations (1.48) and (1.49).
(c) Calculation of real and imaginary parts of complex permittivity using Equations (1.50) and (1.51).
(d) Finally the complex permittivity is fitted by means of a suitable model.

The complex permittivity spectra for both components can be expressed as a sum of quasi-harmonic damped oscillators and ε' and ε'' are then given by [114]

$$\varepsilon'(\nu) = \varepsilon_\infty + \sum_j 4\pi\rho_j \nu_j^2 \frac{\nu_j^2 - \nu^2}{\left(\nu_j^2 - \nu^2\right)^2 + \gamma_j^2 \nu^2} \tag{1.52}$$

$$\varepsilon''(\nu) = \sum_j 4\pi\rho_j \nu_j^2 \frac{\gamma_j \nu}{\left(\nu_j^2 - \nu^2\right)^2 + \gamma_j^2 \nu^2} \tag{1.53}$$

This sum is all over j resonances (i.e., oscillators describing phonons) in the spectrum. The dispersion parameters are $4\pi\rho_j = \Delta\varepsilon_j {\nu_j}^2$ is the strength of the oscillator, where $\Delta\varepsilon_j$ marks the contribution of the jth mode to the static permittivity, γ_j = width (phonon damping), and ν_j = resonant frequency (phonon eigenfrequency). For the $\nu \ll \nu_j$ condition (microwave region) Equations (1.52) and (1.53) can be written in the form:

$$\varepsilon' = e_\infty + 4\pi\rho_j \quad \text{for } \nu \ll \nu_j \tag{1.54}$$

$$\varepsilon''(\nu) \propto V \sum_j \frac{4\pi\rho_j\gamma_j}{\nu_j^2} \tag{1.55}$$

This means that the permittivity is independent of frequency and the dielectric loss ε'' is proportional to frequency at frequencies much below the phonon frequencies ν_j, which lies in the THz range. The $\varepsilon_\infty$is the permittivity caused by electronic polarization at higher frequencies and can be obtained using the frequency independent middle-infrared reflectivity by the equation [118]

$$\varepsilon_\infty = \frac{\left(1 + \sqrt{R}\right)^2}{\left(1 - \sqrt{R}\right)^2} \tag{1.56}$$

The normal incidence of reflectivity is given by Fresnel formula:

$$R = \frac{(n-1)^2 + k^2}{(n+1)^2 + k^2} \tag{1.57}$$

The phonon parameters can be obtained by K-K analysis. Each peak in the plot ε'' versus frequency obtained by the K-K analysis corresponds to a phonon frequency ν_j and γ_j is given by the frequency half-width of the ε_j'' peak. The oscillator strength is determined by:

$$4\pi\rho_j = \frac{\gamma_j \varepsilon_j''}{\nu_j} \tag{1.58}$$

Complex permittivity can be calculated by direct fitting of the experimental reflectivity spectra using the formulas in Equations (1.53) and (1.54) and

$$R = \left(\frac{\left(\sqrt{\varepsilon} - 1\right)}{\left(\sqrt{\varepsilon} + 1\right)} \right)^2 \tag{1.59}$$

The simulation process is done in the following way:

(a) Fix ν_j and γ_j and adjust ρ_j to give the correct width of the reflection band.
(b) Fix ν_j and ρ_j and adjust γ_j to give the correct maximum reflectivity.
(c) ν_j is adjusted to align the fitted curve with the experimental.

Once the best fit is obtained, tan δ can be determined:

$$\tan\delta = \frac{\varepsilon''}{\varepsilon'} = \frac{\sum_j 4\pi\rho_j \nu_j^2 \frac{\gamma_j \nu}{\left(\nu_j^2 - \nu^2\right)^2 + \gamma_j^2 \nu^2}}{\varepsilon_\infty + \sum_j 4\pi\rho_j \nu_j^2 \frac{\nu_j^2 - \nu^2}{\left(\nu_j^2 - \nu^2\right)^2 + \gamma_j^2 \nu^2}} \tag{1.60}$$

At low frequencies $\nu \ll \nu_j$ [117] we obtain

$$\tan\delta = \frac{\sum_j 4\pi\rho_j \frac{\gamma_j \nu}{\nu_j^2}}{\varepsilon_\infty + \sum_j 4\pi\rho_j} \tag{1.61}$$

Equation (1.61) shows that tan δ is linearly frequency dependent.

The far-infrared spectroscopy (FIR) and terahertz transmission spectroscopy are useful methods used to estimate the intrinsic losses [119, 120]. It was reported as early as 1962 that experimental ε'' is proportional to the frequency well below the phonon frequencies ($f \leq 10^{12}$ Hz) [121]. The lattice absorption is the dominant loss mechanism at high frequencies [121, 122] and several authors extrapolated the data at high frequencies obtained by FIR and SMM to the microwave frequency range [120, 123]. Several authors [116, 118, 124–129] estimated the dielectric constant and dielectric loss tangent of materials by analyzing the FIR reflectivity data using the K-K analysis and classical dispersion theory. They found reasonable agreement between the ε_r obtained by the spectroscopic method with that measured by microwave methods. However, the loss tangents measured by microwave methods were found to be higher than those obtained by the far-infrared method. In the loss tangent obtained by microwave methods is the sum of intrinsic and extrinsic dielectric losses. The presence of porosity and crystal defects contribute to the loss factor and the spectroscopic methods give only the intrinsic loss factor. Thus it is possible by the far-infrared and

SMM method to find the lowest loss factor in a particular material, which in turn is helpful when optimizing the ceramic preparation to get a low-loss material and to reduce extrinsic losses. The relative influence of defects on losses decreases with increasing frequency [126]. Hence their influence cannot be measured in the optical frequency range. This enables one to estimate the order of magnitude of intrinsic microwave losses from IR reflectivity on new materials without much processing. Unlike the microwave losses, the IR reflectivity of dense ceramics is less sensitive to sample preparation (i.e., extrinsic losses contribute only slightly to IR spectra). Hence the IR spectroscopic method can be successfully and simply used for estimating the intrinsic microwave losses and dielectric constants of new materials [120, 124, 126]. Nevertheless, it should be stressed that the accuracy of the far-IR (FIR) experiment is rather limited. Therefore it is necessary to combine FIR reflectivity studies with SMM or THz measurements, which are more sensitive than FIR reflectivity on small dielectric losses below phonon frequencies.

The fundamental loss mainly corresponds to the absorption of the energy quantum of the electromagnetic field $\hbar\omega$ ($\omega = 2\pi\nu$ is the AC field frequency) in a collision process with thermal phonons, which have much higher energies [15]. Under such a situation, the absorption of $\hbar\omega$ of energy corresponds to three fundamental loss mechanisms: three quantum, four quantum, and quasi-Debye mechanisms. The three quantum process involves an $\hbar\omega$ quantum and two phonons [15, 130, 131]. The four quantum mechanism corresponds to the field quantum absorption processes involving three phonons. The application of a DC field to a centrosymmetric crystal breaks its central symmetry and therefore gives rise to a quasi-Debye mechanism [15, 130].

In centrosymmetric materials, the crystalline symmetry permits only three quantum and four quantum mechanisms. However, in non-centrosymmetric materials all the three mechanisms are allowed and the quasi-Debye mechanism is dominant for the intrinsic loss. As the ε_r increases, the dielectric loss also increases. For the intrinsic loss mechanism in cubic centrosymmetric crystals, the real ε' and imaginary ε'' are related by $\varepsilon'' \propto \varepsilon^x$, where $x = 2.5$ to 5 [130]. The role of intrinsic losses at microwave frequencies increases with increasing ε_r.

Petzelt and co-workers [120, 123–126, 129, 132, 133] made measurements on many microwave ceramic materials in the IR and SMM (submillimeter) range using FTIR and a backward wave oscillator (BWO) and/or time-resolved THz spectroscopy. The extrapolated losses from the THz to MW range (using $\varepsilon'' \propto \omega$) were compared with those measured directly by microwave methods. It was found in many cases that the extrapolated loss factors were much lower than those measured by microwave methods, indicating that the proportionality $\varepsilon'' \propto \omega$ is not satisfied. The microwave measurements are very sensitive to extrinsic loss depending on the ceramic processing, whereas the spectroscopic methods are not (i.e., extrinsic losses contribute only slightly into dielectric losses in the THz range). The difference in loss factor between those extrapolated from SMM and the microwave methods is attributed to the extrinsic loss factor.

For well-processed ceramics, the model predicts the simple proportionality for intrinsic losses $\varepsilon'' \propto \omega$ (or Qf is a constant), which is usually obeyed, due the minimization of extrinsic losses. However, is not usual to use the extrapolation of the damped harmonic oscillator models down to the microwave range, because it assumes frequency-independent phonon damping, which is not necessary. This is explained by microscopic phonon transport theory [15, 126, 134], which indicates that the simple damped oscillator model with

frequency-independent damping is valid only in the vicinity of phonon eigenfrequencies and the microwave frequencies lie 3–4 orders of magnitude below the phonon frequencies. Nevertheless, far-infrared spectroscopy was used frequently (together with THz spectroscopy) [128, 133, 134] for estimation of intrinsic microwave dielectric losses, and it was shown that the linear extrapolation from the THz to MW range works quite well, although there is no exact detailed theoretical reason for it.

The temperature dependence for dielectric losses of two phonon difference decay processes dominate at room temperature and near the Debye temperature (T_D) in the microwave range far below the eigenfrequencies and therefore $\varepsilon'' \propto \omega T^2$. At low temperatures, the ε'' temperature dependence is very strong, which differs from the classical damped oscillator model $\varepsilon'' \propto \omega T$. The difference is attributed to the presence of extrinsic sources of losses that are strongly frequency dependent [120, 126].

1.9 Factors Affecting Dielectric Loss

The presence of moisture or humidity affects the tan δ [20, 135]. The microwave measurements are usually done in an air-conditioned room in order to minimize its effects and the samples should be heated in an oven to remove the moisture before starting the experiments. The material should also contain the lowest possible concentration of dipoles and charge carriers with the lowest possible mobility to possess low loss [136]. Several technically important insulating materials are far from high purity and often contain deliberate or accidental admixtures of substances that are necessary for their processing. These impurities may cause disordered charge distributions in the crystal lattice, leading to loss [136]. Schlömann [136] reported that in ionic non-conducting crystals, the loss tangent increases when the ions are distributed in such a disorderly way that they break the periodic arrangement of atoms in the crystal. The loss tangent depends strongly on the spatial correlation between charge deviations. Further, Schlömann reported that the loss tangent is negligible if the disordered charge distribution in the crystal maintains the charge neutrality within a short range of the order of lattice constant. The intrinsic quality factor (Q_i = 1/tan δ) of any given material will vary with the frequency of measurements. For many materials, the dielectric loss tangent almost linearly increases as the frequency increases. Hence often the intrinsic quality factor (1/tan δ) is reported as ($Q_i f = f$/tan δ, in GHz) since this value is the first approximation constant. The assumption that the value of $Q_i f$ is constant is satisfied for the well-densified ceramics in a certain limited frequency range. In practice, samples measured at higher frequencies (5–12 GHz) always give higher $Q_i f$ values than the same material measured at lower frequencies of 1–3 GHz. Recently Li and Chen reported [137] that the product Qf is frequency dependent and increases with frequency. The frequency dependence of the Qf value is attributed to the presence of defects-induced extrinsic dielectric loss. It may be noted that larger samples resonating at lower frequencies statistically contain more imperfections than smaller ceramic disks resonating at higher frequencies. This difference may be related to ceramic processing. The presence of porosity decreases the quality factor due to the presence of moisture in the pores. Hence porous samples show an increase in $Q_i f$ on warming up due to the escape of moisture.

Gurevich and Tagantsev [15, 16] investigated the fundamental theory of intrinsic losses and reported that the lower limit of intrinsic losses are found in pure defect-free single

crystals. Several phonon processes contribute to intrinsic losses in a dielectric and their importance depends on the AC field frequency, temperature range. and symmetry of the crystal under consideration. The loss mechanisms are different for a crystal with and without a center of symmetry. Guvevich *et al.* [15, 16] analyzed the lattice anharmonicity for various crystal symmetries and obtained numerical estimates of tan δ of ideal crystals.

For hexagonal symmetry and $T \ll T_D$ (T_D = Debye temperature),

$$\tan\delta = \frac{\eta\omega(kT)^5}{\varepsilon_r \rho v_s^5 h^2 (kT_D)^2} \tag{1.62}$$

and for rhombohedral or cubic symmetry,

$$\tan\delta = \frac{\eta\omega^2(kT)^4}{\varepsilon_r \rho v_s^5 h (kT_D)^2} \tag{1.63}$$

where η is a dimensionless anharmonicity parameter ranging between 1 and 100, ω is the angular frequency, k = Boltzmann constant, T = absolute temperature, v_s = sound velocity, T_D = Debye temperature, and ρ is the density.

For the hexagonal symmetry, tan δ decreases rapidly with a decrease of temperature as T^5 and in centrosymmetric crystals as T^4. The decrease in tan δ as a function of temperature in the range 3.5 to 300 K was verified experimentally [17] for three hexagonal sapphire samples of different defect concentrations, as shown in Figure 1.30. The curve (a) is for a sample

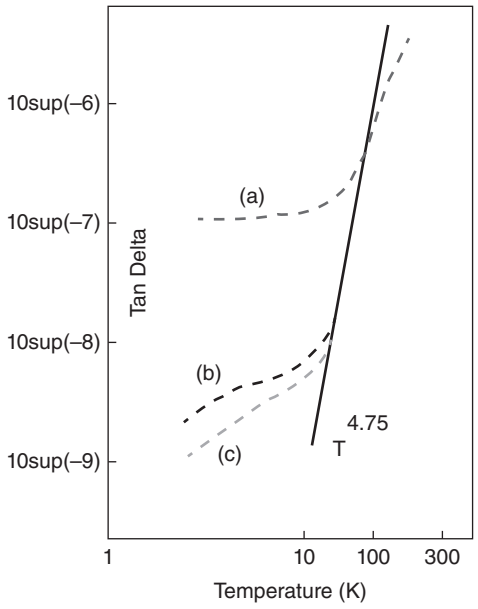

Figure 1.30 *Variation of tan δ of three different sapphire crystals as a function of temperature on cooling: (a) crystal with disorientation, (b) crystal grown at the rate of 8 mm/h, and (c) crystal grown at the rate of 4 mm/h. Source: Adapted from Braginsky* et al. *1987 [17].*

that contained a block structure with a disorientation of 1°, the curve (b) corresponds to a sample grown at the rate of 8 mm/h, and curve (c) at the rate of 4 mm/h. It is observed that curve (a) shows a higher loss due to the larger defect concentration. It is also observed in Figure 1.30 that tan δ decreased with decreasing temperature. All samples showed a linear section in the temperature range 50 to 300 K, where tan $\delta \sim T^{\alpha}$ ($\alpha = 4.75$). This value is reported as the lower limit of the dielectric losses at a given frequency, which is independent of the variation of the defect structure and is of fundamental origin [17]. At temperatures $T < 50$ K, the value of tan δ is greatly affected by the level of crystal perfection. Bragisnsky *et al.* [17] extrapolated from the experimentally obtained tan δ–temperature plot (Figure 1.30) to predict a tan $\delta \sim 5 \times 10^{-15}$ at 4 K at 10 GHz for a defect-free crystal. This corresponds to a Q value of about 2×10^{14}, which can be considered as the upper limit of the quality factor in a perfect sapphire crystal. There is no predictive theory to account for the microwave loss in dielectric ceramics. Hence the approach to find new dielectric resonator materials is largely done by the trial and error method involving preparing and testing a large number of samples.

1.10 Measurement of Temperature Coefficient of Resonant Frequency

The temperature coefficient of resonant frequency (τ_f) is the parameter that determines the thermal stability of the resonator. The τ_f indicates how much the resonant frequency drifts with a change in the temperature. The electronic devices based on microwave resonators are required to have τ_f values close to zero. Microwave circuits will normally have some low characteristics τ_f, so the resonator components that are introduced into them are required to compensate for the inherent drift. For this reason the τ_f values of resonators are typically non-zero but have some low finite values. The origin of τ_f is related to the linear expansion coefficient α_L of the resonator and its dielectric constant variation with temperature [8]. Mathematically the relationship is

$$\tau_f = -\alpha_L - \frac{\tau_\varepsilon}{2} \tag{1.64}$$

where τ_ε is the temperature coefficient of the permittivity and α_L is the linear thermal expansion coefficient of the dielectric material, which is usually positive.

In practice, the Equation (1.64) is valid for 100% electric energy storage in the sample and the thermal expansion of the metal cavity enclosing the DR is negligible. For an ideal resonator the temperature coefficient of resonant frequency (τ_f) should be near zero. Hence from Equation (1.64) for a zero τ_f, τ_ε should have twice the value of α_L and should be negative. Since resonators are used in communication systems, temperature stability is an important factor and should be close to zero. For most of the electronic ceramic materials α_L is about +10 ppm/°C, indicating the significant influence of τ_ε on τ_f.

Experimentally τ_f is measured by following the drift in the resonant peak frequency f as the temperature is slowly varied. In order to measure τ_f, the dielectric resonator is kept end-shorted between two copper plates under the Courtney setup. This is then kept inside a temperature-controlled oven. The E-field probe is kept near the DR in such a way as to get resonance. The TE_{011} mode is identified and the setup is then slowly heated ($\sim$ 1 °C/minute) in the range 25 to 80 °C. The probe of the thermocouple is kept just inside the oven so that

it does not disturb the resonant frequency. Shift of the resonant frequency as a result of heating in the reflection mode is noted using a network analyzer when the temperature is steady. The variation of resonant frequency is plotted as a function of temperature. The τ_f is calculated from the slope of the curve using

$$\tau_f = \frac{f_{80} - f_{25}}{f_{25}\,(80 - 25))} = \frac{1}{f}\frac{\Delta f}{\Delta T} \times 10^6 \tag{1.65}$$

The τ_f is expressed as parts per million per degree Celsius (ppm/°C).

The τ_f can also be measured by the cavity method used for measuring the quality factor. The thermal expansion of the cavity during heating limits the accuracy of the method. However, use of a cavity made of invar can minimize the inaccuracy. In fact, thermal expansion of the cavity is negligibly small for whispering gallery modes and also for a $TE_{01\delta}$ mode resonant structure if permittivity of the sample is large and the sample is situated away from all cavity walls. The τ_f is related to thermal expansion and relative permittivity by the relation (1.64). The temperature coefficient of the dielectric constant τ_ε is of considerable interest to users of dielectric substrates. This can be obtained by the parallel plate capacitor method using an LCR meter at low frequency (e.g., 1 MHz) and heating the sample. From the ε_r noted at different temperatures the τ_ε can be obtained. At microwave frequency, one can obtain τ_ε from the value of τ_f and α_L and using Equation (1.64). The temperature coefficient of resonance frequency and the Q-factor are quantities that characterize the resonator and depend not only on the properties of the ceramic sample but also on the properties of other parts of the resonance system.

The high dielectric loss ceramics cannot enable the measurements of τ_f due to the fact that monitoring the TE_{011} mode is not possible. Ceramics with a high dielectric loss do not have the TE_{011} mode clearly detectable, which leads to difficulties of taking the measurements of τ_f of this kind of material. For these kinds of materials another method for τ_f measurements was developed by Silva *et al.* [138]. This new procedure uses an experimental setup where the dielectric loss would not affect the mode identification. The experimental setup for a dielectric resonator antenna (DRA) showed it to be an ideal setup for this measurement, where the peaks are very well defined modes and the high dielectric loss would not affect the mode identification. The experiment setup consists of a DRA, fed laterally by an SMA probe, coupled to a ceramic oven, as shown in Figure 1.31.

The dominant mode for this DRA is the $HE_{11\delta}$ mode and the measurement of τ_f of any sample is made to accomplish the shift of the resonant frequency of $HE_{11\delta}$ mode with increasing temperature (see Figure 1.32). For samples that have a high dielectric loss, the traditional measurements for the Hakki–Coleman setup do not allow the TE_{011} mode visualization to be obtained, due to the convolution of the TE_{011} mode with adjacent modes (see Figure 1.33). In this case the τ_f could not be obtained. Figure 1.33 shows a measurements of a high dielectric loss ceramic by the SFS method [138], where the new methodology to enable measurements for this kind ceramic can be seen.

1.11 Tuning of the Resonant Frequency

The resonant frequency of a resonator depends on the resonator surroundings, relative permittivity, and the sample dimensions. It is possible to tune the frequency of a particular

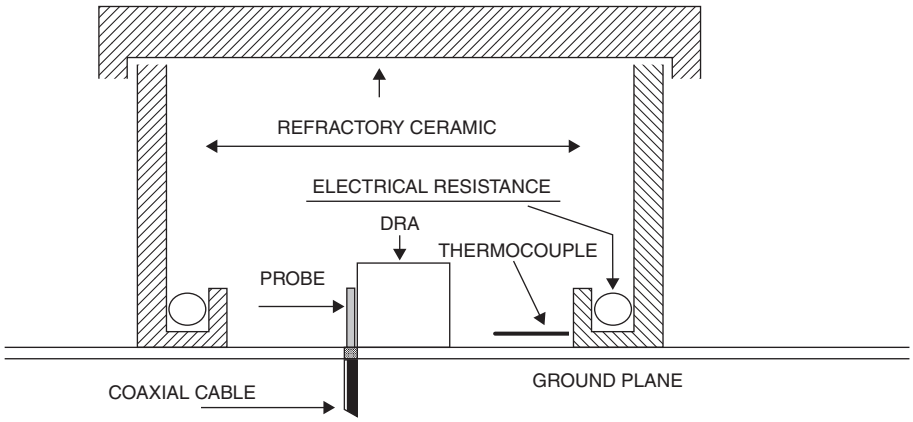

Figure 1.31 *Experimental setup for τ_f measurements by an $HE_{11\delta}$ frequency shift.*

resonator [139–142] by a tuning plate, dielectric plug, or a dielectric disk, as shown in Figure 1.34. The dielectric plug or dielectric disk tuning may decrease the quality factor only by less than 5%, whereas plate tuning leads to a considerable decrease of the Q-factor. When a metallic tuner is introduced, the resonant frequency will increase as the tuner approaches the DR, but if a dielectric tuner is used then the resonant frequency will decrease. By these methods, a change in resonant frequency up to about 15% can be achieved.

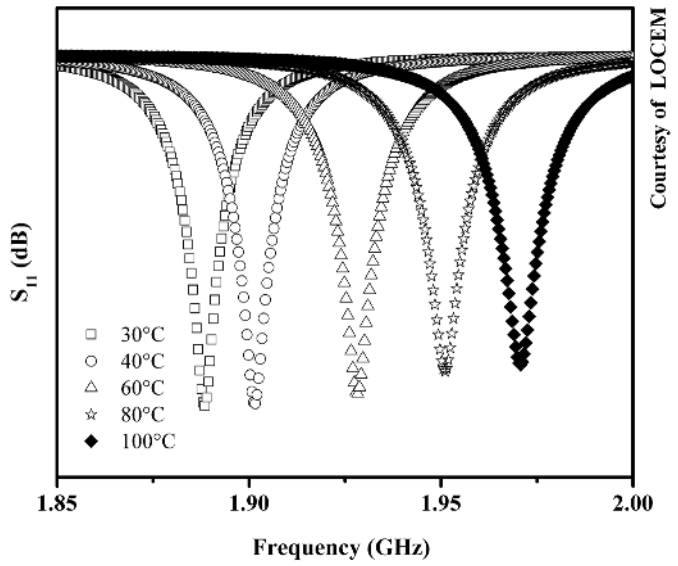

Figure 1.32 *The frequency displacement of $HE_{11\delta}$ mode frequency as a function of temperature variation.*

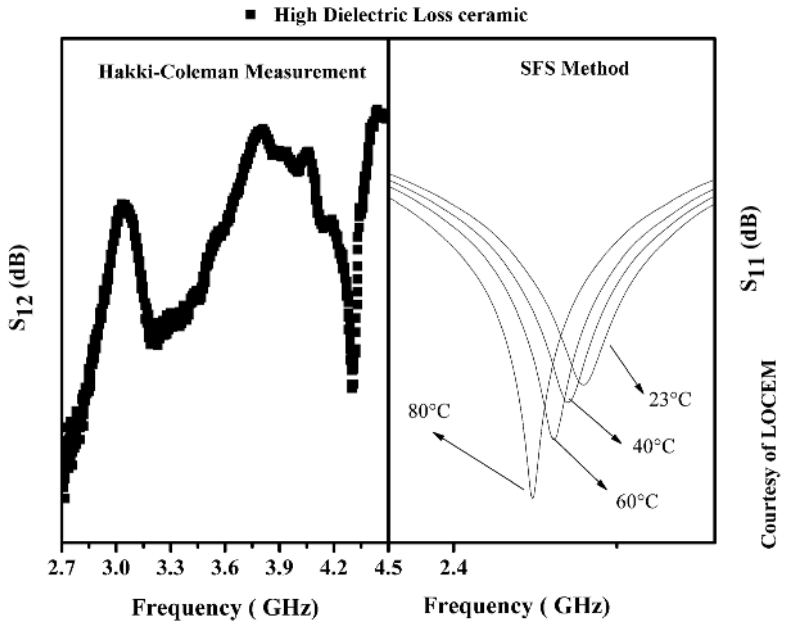

Figure 1.33 *The frequency profile of Hakki–Coleman measurements of a high dielectric loss ceramic in comparison with the measurements using the SFS method.*

However, when using a metallic plate tuner, the tuning range may be limited to only a few percent in order to avoid serious degradation of the Q-factor and τ_f. Another way to tune the frequency is by changing the physical size of the DR by machining and reducing the thickness or diameter of the DR. It is also possible to tune the frequency by increasing the size of the resonator by attaching a small piece of low-loss ceramic to the DR using low-loss glue. The resonators can be mounted to a ceramic substrate using a small drop of low-loss adhesive such as cyanoacrylic. Recently Petrov and Alford [143] reported fast resonant frequency tuning in dielectric resonators by incorporating a thick film of $Ba_{1-x}Sr_xTiO_3$.

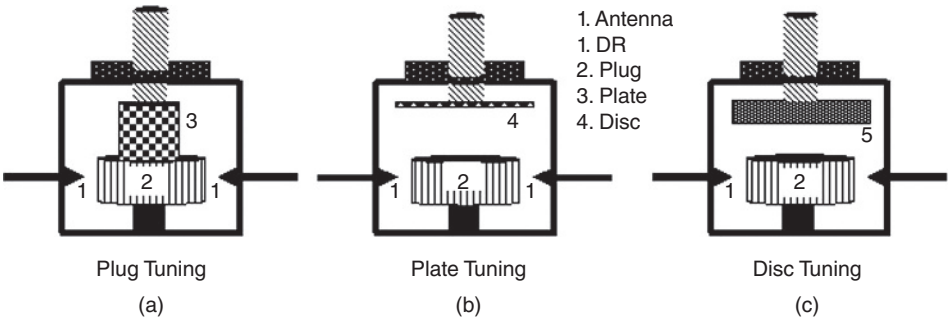

Figure 1.34 *Schematic diagrams showing tuning of the resonant frequency: (a) plug tuning, (b) plate tuning, and (c) disk tuning.*

References

1. Rayleigh, Lord (1987) On the passage of wave through tubes, or the vibration of dielectric cylinders. *Philosophical Magazine*, **43**, 125–132.
2. Richtmyer, R.D. (1939) Dielectric resonators. *Journal of Applied Physics*, **10** (6), 391.
3. Okaya, A. and Barash, L. (1962) The dielectric microwave resonator. *Proceedings of the IRE*, **50** (10), 2081–2092.
4. Okaya, A. (1962) The rutile microwave resonator. *Proceedings of the IRE*, **48**, 1921.
5. Cohn, S.B. (1965) Microwave filters containing high-Q dielectric resonators. *G-MTT Symposium Digest*, **MTT002**, 49–54.
6. Sebastian, M.T. (2010) *Dielectric Materials for Wireless Communication*, Elsevier Science, 688 pp.
7. Sebastian, M.T., Ubic, R., and Jantunen, H. (2015) Low-loss dielectric ceramic materials and their properties. *International Materials Reviews*, **60** (7), 392–412.
8. Kajfez, D. and Guillon, P. (1998) *Dielectric Resonators*, Noble Publishing Corporation, 547 pp.
9. Schwartz, B. (1984) Microwlwctronic packaging II. *American Ceramic Society Bulletin*, **63**, 577–581.
10. Tummala, R.R. (1991) Ceramic and glass–ceramic packaging in the 1990s. *Journal of the American Ceramic Society*, **74** (5), 895–908.
11. Moulson, A.J. and Herbert, J.M. (2003) *Electroceramics: Materials, Properties, Applications*, John Wiley & Sons.
12. Raghavan, V. (2004) *Materials Science and Engineering: A First Course*, PHI Learning, 430 pp.
13. Burfoot, J.C. (1967) *Ferroelectrics: An Introduction to the Physical Principles*, London: D. Van Nostrand Company, London 261 pp.
14. Krupka, J. (2006) Frequency domain complex permittivity measurements at microwave frequencies. *Measurement Science and Technology*, **17** (6), R55–R70.
15. Gurevich, V.L. and Tagantsev, A.K. (1991) Intrinsic dielectric loss in crystals. *Advances in Physics*, **40** (6), 719–767.
16. Gurevich, V.-L. and Tagantsev, A.K. (1986) Intrinsic dielectric loss in crystals: low temperature. *Soviet Physics JETP*, **64**, 10.
17. Braginsky, V.B., Ilchenko, V.S., and Bagdassarov, K.S. (1987) Experimental observation of fundamental microwave absorption in high-quality dielectric crystals. *Physics Letters A*, **120** (6), 300–305.
18. Chen, L.F., Ong, C.K., Neo, C.P., Varadan, V.V., and Varadan, V.K. (2004) *Microwave Electronics: Measurement and Materials Characterization*, John Wiley & Sons, 552 pp.
19. Hakki, B.W. and Coleman, P.D. (1960) A dielectric resonator method of measuring inductive capacities in the millimeter range. *IEEE Transactions on Microwave Theory and Techniques*, **8** (4), 402–410.
20. Courtney, W.E. (1970) Analysis and evaluation of a method of measuring the complex permittivity and permeability microwave insulators. *IEEE Transactions on Microwave Theory and Techniques*, **18** (8), 476–485.
21. Kobayashi, Y. and Katoh, M. (1985) Microwave measurement of dielectric properties of low-loss materials by the dielectric rod resonator method. *IEEE Transactions on Microwave Theory and Techniques*, **33** (7), 586–592.
22. Kobayashi, Y. and Tanaka, S. (1980) Resonant modes of a dielectric rod resonator short-circuited at both ends by parallel conducting plates. *IEEE Transactions on Microwave Theory and Techniques*, **28** (10), 1077–1085.
23. Cohn, S.B. and Kelly, K.C. (1966) Microwave measurement of high-dielectric- constant materials. *IEEE Transactions on Microwave Theory and Techniques*, **14** (9), 406–410.
24. Ginzton, E.L. (2012) *Microwave Measurements*, Literary Licensing, LLC, 534 pp.
25. Vanzura, E.J. and Rogers, J.E. (1991) Resonant circuit model evaluation using reflected S-parameter data, in *Conference Record. IEEE Instrumentation and Measurement Technology Conference*, IEEE, pp. 150–155.

26. Rebsch, D.L., Webb, D.C., Moore, R.A., and Cowlishaw, J.D. (1965) A mode chart for accurate design of cylindrical dielectric resonators (correspondence). *IEEE Transactions on Microwave Theory and Techniques*, **13** (4), 468–469.
27. International Standard IEC 61338-1–4, 1st edn (2005-11) Waveguide type dielectric resonators. Part 1–4: General information and test conditions – Measurement method of complex permittivity for dielectric resonator materials at millimetre-wave frequency. International Electrotechnical Commission, Geneva, Switzerland.
28. Wheless, P. and Kajfez, D. (1985) The use of higher resonant modes in measuring the dielectric constant of dielectric resonators. *MTT-S International Microwave Symposium Digest*, **MTT005**, 473–476.
29. Kobayashi, Y. and Tamura, H. (1994) Round Robin Test on a dielectric resonator method for measuring complex permittivity at microwave frequency (Special Issue on Measurement Techniques for Microwave/Millimeter Wave). *IEICE Transactions on Electronics, The Institute of Electronics, Information and Communication Engineers*, **77** (6), 882–887.
30. Pospieszalski, M.W. (1977) On the theory and application of the dielectric post resonator (Short Papers). *IEEE Transactions on Microwave Theory and Techniques*, **25** (3), 228–231.
31. Takagi, H., Fujinami, N., Tamura, H., and Wakino, K. (1992) Measurement accuracy of complex permittivity in the dielectric rod resonator method. *Japanese Journal of Applied Physics*, **31** (Part 1, No. 9B), 3269–3271.
32. Krupka, J., Derzakowski, K., Riddle, B., and Baker-Jarvis, J. (1998) A dielectric resonator for measurements of complex permittivity of low loss dielectric materials as a function of temperature. *Measurement Science and Technology*, **9** (10), 1751–1756.
33. Leong, K., Mazierska, J., and Krupka, J. (1997) Measurements of unloaded Q-factor of transmission mode dielectric resonators, in *IEEE MTT-S International Microwave Symposium Digest*, IEEE, pp. 1639–1642.
34. Tamura, H., Matsumoto, H., and Wakino, K. (1989) Low temperature properties of microwave dielectrics. *Japanese Journal of Applied Physics*, **28** (S2), 21.
35. Krupka, J., Huang, W.-T., and Tung, M.-J. (2005) Complex permittivity measurements of low-loss microwave ceramics employing higher order quasi TE 0 np modes excited in a cylindrical dielectric sample. *Measurement Science and Technology*, **16** (4), 1014–1020.
36. Valant, M., Suvorov, D., and Maček S. (1996) Measurement error analysis in the determination of microwave dielectric properties using cavity reflection method. *Ferroelectrics*, **176** (1), 167–177.
37. Scott, A.W. (1993) *Understanding Microwaves*, John Wiley & Sons, Inc., New York.
38. Khanna, A. and Garault, Y. (1983) Determination of loaded, unloaded, and external quality factors of a dielectric resonator coupled to a microstrip line. *IEEE Transactions on Microwave Theory and Techniques*, **31** (3), 261–264.
39. Wait, J.R. (1967) Electromagnetic whispering gallery modes in a dielectric rod. *Radio Science*, **2** (9): 1005–1017.
40. Cros, D. and Guillon, P. (1990) Whispering gallery dielectric resonator modes for W-band devices. *IEEE Transactions on Microwave Theory and Techniques*, **38** (11), 1667–1674.
41. Krupka, J., Cros, D., Aubourg, M., and Guillon, P. (1994) Study of whispering gallery modes in anisotropic single-crystal dielectric resonators. *IEEE Transactions on Microwave Theory and Techniques*, **42** (1), 56–61.
42. Blair, D.G., Woode, R.A., Tobar, M.E., and Ivanov, E.N. (1994) Measurement of dielectric loss tangent of alumina at microwave frequencies and room temperature. *Electronics Letters*, **30** (25), 2120–2122.
43. Ivanov, E.N., Blair, D.G., and Kalinichev, V.I. (1993) Approximate approach to the design of shielded dielectric disk resonators with whispering-gallery modes. *IEEE Transactions on Microwave Theory and Techniques*, **41** (4), 632–638.
44. Tobar, M.E. and Mann, A.G. (1991) Resonant frequencies of higher order modes in cylindrical anisotropic dielectric resonators. *IEEE Transactions on Microwave Theory and Techniques*, **39** (12), 2077–2082.

45. Krupka, J., Derzakowski, K., Abramowicz, A., Tobar, M.E., and Geyer, R.G. (1999) Use of whispering-gallery modes for complex permittivity determinations of ultra-low-loss dielectric materials. *IEEE Transactions on Microwave Theory and Techniques*, **47** (6), 752–759.
46. Krupka, J. (1996) Measurements of the complex permittivity of microwave circuit board substrates using split dielectric resonator and reentrant cavity techniques, in *Seventh International Conference on Dielectric Materials, Measurements and Applications*, IEEE, pp. 21–24.
47. Krupka, J., Gregory, A.P., Rochard, O.C., Clarke, R.N., Riddle, B., and Baker-Jarvis, J. (2001) Uncertainty of complex permittivity measurements by split-post dielectric resonator technique. *Journal of the European Ceramic Society*, **21** (15), 2673–2676.
48. Krupka, J. (2013) Contactless methods of conductivity and sheet resistance measurement from semiconductors, conductors and superconductors. *Measurement Science and Technology*, **24**, 062001.
49. Kent, G. (1988) An evanescent-mode tester for ceramic dielectric substrates. *IEEE Transactions on Microwave Theory and Techniques*, **36** (10), 1451–1454.
50. Krupka, J. (2003) Precise measurements of the complex permittivity of dielectric materials at microwave frequencies. *Materials Chemistry and Physics*, **79** (2–3), 195–198.
51. Parkash, A., Vaid, J.K., and Mansingh, A. (1979) Measurement of dielectric parameters at microwave frequencies by cavity-perturbation technique. *IEEE Transactions on Microwave Theory and Techniques*, **27** (9), 791–795.
52. Von Aulock, W. and Rowen, J.H. (1957) Measurement of dielectric and magnetic properties of ferromagnetic materials at microwave frequencies. *Bell System Technical Journal*, **36** (2), 427–448.
53. Spencer, E., Lecraw, R., and Reggia, F. (1956) Measurement of microwave dielectric constants and tensor permeabilities of ferrite spheres. *Proceedings of the IRE*, **44** (6), 790–800.
54. Artman, J.O. and Tannenwald, P.E. (1953) Measurement of permeability tensor in ferrites. *Physical Review*, **91** (4), 1014–1015.
55. Slater, J.C. (1946) Microwave electronics. *Reviews of Modern Physics*, **18** (4), 441–512.
56. Daiqing, Li, Free, C.E., Pitt, K.E.G., and Barnwell, P.G. (2001) A simple method for accurate loss tangent measurement of dielectrics using a microwave resonant cavity. *IEEE Microwave and Wireless Components Letters*, **11** (3), 118–120.
57. Bussey, H.E. and Steinert, L.A. (1958) Exact solution for a gyromagnetic sample and measurements on a ferrite. *IEEE Transactions on Microwave Theory and Techniques*, **6** (1), 72–76.
58. Ohlsson, P.O.R. (1975) Theory for and experiments with a TM_{02n} applicator. *Journal of Microwave Power and Electromagnetic Energy (JMPEE)*, **10** (3), 271–280.
59. Parry, J.V.L. (1951) The measurement of permitivity and power factor of dielectrics at frequencies from 300 to 600 Mc/s. *Proceedings of the IEE – Part III: Radio and Communication Engineering*, **98** (54), 303–311.
60. Kaczkowski, A. and Milewski, A. (1980) High-accuracy wide-range measurement method for determination of complex permittivity in reentrant cavity: Part A – Theoretical analysis of the method. *IEEE Transactions on Microwave Theory and Techniques*, **28** (3), 225–228.
61. Karpova, O.V. (1959) On an absolute method of measurement of dielectric properties of a solid using shaped resonator. *Sovet Physics*, **1**, 220–228.
62. Horner, F., Taylor, T.A., Dunsmuir, R., *et al.* (1946) Resonance methods of dielectric measurement at centimetre wavelengths. *Journal of the Institution of Electrical Engineers – Part III: Radio and Communication Engineering*, **93** (21), 53–68.
63. Cook, R.J., Jones, R.G., and Rosenberg, C.B. (1974) Comparison of cavity and open-resonator measurements of permittivity and loss angle at 35 GHz. *IEEE Transactions on Instrumentation and Measurement*, **23** (4), 438–442.
64. Stumper, U. (1973) A TE_{01n} cavity resonator method to determine the complex permittivity of low loss liquids at millimeter wavelengths. *Review of Scientific Instruments*, **44** (2), 165.
65. Yu, P.K. and Cullen, A.L. (1982) Measurement of permittivity by jeans of an open resonator. I. Theoretical. *Proceedings of the Royal Society of London. A. Mathematical and Physical Sciences*, **380** (1778), 49–71.

66. Ghodgaonkar, D.K., Varadan V.V., Varadan, V.K. (1989) Free-space method for measurement of dielectric constants and loss tangents at microwave frequencies. *IEEE Transactions on Instrumentation and Measurement*, **38** (3), 789–793.
67. Campbell, C.K. (1978) Free-space permittivity measurements on dielectric materials at millimeter wavelengths. *IEEE Transactions on Instrumentation and Measurement*, **27** (1), 54–58.
68. Amiet, A. and Jewsbury, P. (2000) Free space microwave permittivity and permeability measurements, in *Microwave Conference, 2000 Asia-Pacific Publication*, pp. 445–448.
69. Bartley, P.G. and Begley, S.B. (2005) Improved free-space *S*-parameter calibration. *2005 IEEE Instrumentationand Measurement Technology Conference Proceedings*, **1** (May), 17–19.
70. Cullen, A.L. (1983) Millimeter wave open resonator techniques, Chapter 4, in *Infrared and Millimeter Waves*, vol. **10**, Elsevier, p. 424.
71. Afsar, M.N., Li, X., and Chi, H. (1990) An automated 60 GHz open resonator system for precision dielectric measurements. *IEEE Transactions on Microwave Theory and Techniques*, **38**, (12), 1845–1853.
72. Das, A. and Das, S.K. (2008) *Microwave Engineering*, McGraw-Hill Higher Education, Boston, MA.
73. Born, M., Wolf, E., Bhatia, A.B., *et al.* (2000) *Principles of Optics: Electromagnetic Theory of Propagation, Interference and Diffraction of Light*, Cambridge University Press.
74. Gorshunov, B.P, Volkov, A.A., Prokhorov, A.S, and Spektor, I.E. (2008) Methods of terahertz–subterahertz BWO spectroscopy of conducting materials. *Physics of the Solid State*, **50** (11), 2001–2012.
75. Kozlov, G. and Volkov, A. (1998) Coherent source submillimeter wave spectroscopy, in *Millimeter and Submillimeter Wave Spectroscopy of Solids SE – 3* (ed. G. Grüner), Springer, Berlin and Heidelberg, pp. 51–109.
76. Gorshunov, B., Volkov, A., Spektor, I., *et al.* (2005) Terahertz BWO-Spectrosopy. *International Journal of Infrared and Millimeter Waves*, **26** (9), 1217–1240.
77. Gorshunov, B.P., Prokhorov, A.S., Spektor, I.E., and Volkov, A.A. (2005) Submillimeter spectroscopy of materials with correlated electrons. *Radiophysics and Quantum Electronics*, **48** (10–11), 825–830.
78. Arik, E., Altan, H., and Esenturk, O. (2014) Dielectric properties of ethanol and gasoline mixtures by terahertz spectroscopy and an effective method for determination of ethanol content of gasoline. *The Journal of Physical Chemistry A*, **118** (17), 3081–3089.
79. Beluze, L., Badot, J.C., Weil, R., and Lucas, V. (2006) Broadband dielectric and resistivity spectroscopy of $WO_3 \cdot H_2O$ in the range of $10^3 - 10^{10}$ Hz: particle size effect. *The Journal of Physical Chemistry B*, **110** (14), 7304–7308.
80. Afsar, M.N., Chamberlain, J., and Chantry, G.W. (1976) High-precision dielectric measurements on liquids and solids at millimeter and submillimeter wavelengths. *IEEE Transactions on Instrumentation and Measurement*, **IM-25** (4), 290–294.
81. Choi, M.K, Taylor, K., Bettermann, A., and van der Weide, D.W. (2002) Broadband 10–300 GHz stimulus-response sensing for chemical and biological entities. *Physics in Medicine and Biology*, **47** (21), 3777.
82. Quéffélec, P., Konn, A.-M., Gelin, P., and Mallégol, S. (2003) Experimental demonstration of the nonreciprocity of magnetic composite materials for microwave applications. *Journal of Applied Physics*, **93** (10), 7474.
83. Kanamadi, C.M., Das, B.K., Kim, C.W., *et al.* (2009) Dielectric and magnetic properties of $(x)CoFe_2O_4 + (1 - x)Ba_{0.8}Sr_{0.2}TiO_3$ magnetoelectric composites. *Materials Chemistry and Physics*, **116** (1), 6–10.
84. Brown, E.R., Bjarnason, J.E., Chan, T.L.J., Lee, A.W.M., and Celis, M.A. (2004) Optical attenuation signatures of *Bacillus subtillis* in the THz region. *Applied Physics Letters*, **84** (18), 3438.
85. Khan, U.A., Al-Moayed, N., Nguyen, N., *et al.* (2007) Broadband dielectric characterization of tumorous and nontumorous breast tissues. *IEEE Transactions on Microwave Theory and Techniques*, **55** (12), 2887–2893.
86. Afsar, M.N. and Khan, U. (2005) Measurement of broadband dielectric properties of 10% formalin and 1,4-dioxane using dispersive Fourier transform spectroscopy, in *2005 IEEE Instrumentationand Measurement Technology Conference Proceedings*, IEEE, pp. 925–928.

87. Afsar, M.N., Wang, Y., and Moonshiram, A. (2003) Measurement of transmittance and permittivity of dielectric materials using dispersive Fourier transform spectroscopy. *Microwave and Optical Technology Letters*, **38** (1), 27–30.
88. Kratzenberg, E., Afsar, M.N., and Wang, Y. (2003) Complex permittivity measurements of chicken blood. *Microwave and Optical Technology Letters*, **39** (1), 54–56.
89. Afsar, M.N., Moonshiram, A., and Wang, Y. (2004) Assessment of random and systematic errors in millimeter-wave dielectric measurement using open resonator and Fourier transform spectroscopy systems. *IEEE Transactions on Instrumentation and Measurement*, **53** (4), 899–906.
90. Almoayed, N.N. and Afsar, M.N. (2006) High-resolution absorption coefficient and refractive index spectra of carbon monoxide gas at millimeter and submillimeter wavelengths. *IEEE Transactions on Instrumentation and Measurement*, **55** (4), 1033–1037.
91. Nichols, E.F. and Tear, J.D. (1925) Joining the infra-red and electric-wave spectra. *Astrophysics Journal*, **61**, 17.
92. Auston, D.H., Cheung K.P., and Smith, P.R. (1984) Picosecond photoconducting Hertzian dipoles. *Applied Physics Letters*, **45** (3), 284.
93. Dahl, C., Grüner, G., Genzel, L., *et al.* (1998) *Millimeter and Submillimeter Wave Spectroscopy of Solids*, Springer, Berlin and Heidelberg, 287 pp.
94. Köhler, R., Tredicucci, A., Beltram, F., *et al.* (2002) Terahertz semiconductor-heterostructure laser. *Nature*, **417** (6885), 156–159.
95. Fattinger, C. and Grischkowsky, D. (1988) Point source terahertz optics. *Applied Physics Letters*, **53** (16), 1480.
96. Zhang, X.-C., Jin, Y., and Ma, X.F. (1992) Coherent measurement of THz optical rectification from electro-optic crystals. *Applied Physics Letters*, **61** (23), 2764.
97. Zheng, X., McLaughlin, C.V., Cunningham, P., and Hayden, L.M. (2007) Organic broadband terahertz sources and sensors. *Journal of Nanoelectronics and Optoelectronics*, **2**, 58–76.
98. Davies, A.G., Burnett, A.D., and Fan, W., *et al.* (2008) Terahertz spectroscopy of explosives and drugs. *Materials Today*, **11** (3), 18–26.
99. Khan, U.A., Nguyen, N., and Afsar, M.N. (2008) Millimeter- and submillimeter-wave dielectric measurements of household powders using Fourier transform spectroscopy. *IEEE Transactions on Instrumentation and Measurement*, **57** (2), 286–293.
100. Lowry, H.H. (1927) The significance of the dielectric constant of a mixture. *Journal of the Franklin Institute*, **203** (3), 413–439.
101. Sebastian, M.T. and Jantunen, H. (2010) Polymer–ceramic composites of 0–3 connectivity for circuits in electronics: a review. *International Journal of Applied Ceramic Technology*, **7**, 415–434.
102. Conger, N.L. (1967) Measurement of dielectric constant and loss factor of powder materials in the microwave region. *Review of Scientific Instruments*, **38** (3), 384.
103. Nelson, S.O. and Kraszewski, A.W. (1998) Sensing pulverized material mixture proportions by resonant cavity measurements. *IEEE Transactions on Instrumentation and Measurement*, **47** (5), 1201–1204.
104. Nelson, S.O. and Bartley, P.G. (1998) Open-ended coaxial-line permittivity measurements on pulverized materials. *IEEE Transactions on Instrumentation and Measurement*, **47** (1), 133–137.
105. Ebara, H., Inoue, T., and Hashimoto, O. (2006) Measurement method of complex permittivity and permeability for a powdered material using a waveguide in microwave band. *Science and Technology of Advanced Materials*, **7** (1), 77–83.
106. Tuhkala, M., Juuti, J., and Jantunen, H. (2013) Method to characterize dielectric properties of powdery substances. *Journal of Applied Physics*, **114** (1), 014108.
107. Gershon, D.L., Calame, J.P., Carmel, Y., *et al.* (1999) Open-ended coaxial probe for high-temperature and broad-band dielectric measurements. *IEEE Transactions on Microwave Theory and Techniques*, **47** (9), 1640–1648.
108. Murata, K., Hanawa, A., and Nozaki, R. (2005) Broadband complex permittivity measurement techniques of materials with thin configuration at microwave frequencies. *Journal of Applied Physics*, **98** (8), 084107.

109. Tuhkala, M., Juuti, J., and Jantunen, H. (2014) An indirectly coupled open-ended resonator applied to characterize dielectric properties of $MgTiO_3$–$CaTiO_3$ powders. *Journal of Applied Physics*, **115** (18), 184101.
110. Tuhkala, M., Juuti, J., and Jantunen, H. (2013) Use of an open-ended coaxial cavity method to characterize powdery substances exposed to humidity. *Applied Physics Letters*, **103** (14), 142907.
111. Bruggeman, D.A.G. (1935) Berechnung verschiedener physikalischer Konstanten von heterogenen Substanzen. I. Dielektrizitätskonstanten und Leitfähigkeiten der Mischkörper aus isotropen Substanzen. *Annalen der Physik*, **416** (7), 636–664.
112. Looyenga, H. (1965) Dielectric constants of heterogeneous mixtures. *Physica*, **31** (3), 401–406.
113. Tuhkala, M., Juuti, J., and Jantunen, H. (2014) Determination of complex permittivity of surfactant treated powders using an open-ended coaxial cavity resonator. *Powder Technology*, **256**, 140–145.
114. Spitzer, W.G., Miller, R.C., Kleinman, D.A., and Howarth, L.E. (1962) Far infrared dielectric dispersion in $BaTiO_3$, $SrTiO_3$ and TiO_2. *Physical Review*, **126** (5), 1710–1721.
115. Spitzer, W.G. and Kleinman, D.A. (1961) Infrared lattice bands of quartz. *Physical Review*, **121** (5), 1324–1335.
116. Perry, C.H., McCarthy, D.J., and Rupprecht, G. (1965) Dielectric dispersion of some perovskite zirconates. *Physical Review*, **138** (5A), A1537–A1538.
117. Kudesia, R., McHale, A.E, Condrate, R.A., and Snyder, R.L. (1993) Microwave characteristics and far-infrared reflection spectra of zirconium tin titanate dielectrics. *Journal of Materials Science*, **28** (20), 5569–5575.
118. Wakino, K., Sagala, D.A., and Tamura, H. (1985) Far infrared reflection spectra of $Ba(ZnTa)O_3$–$BaZrO_3$ dielectric resonator material. *Japanese Journal of Applied Physics*, **24** (S2), 1042.
119. Grischkowsky, D., Keiding, S., Exter, M. van, and Fattinger, C. (1990) Far-infrared time-domain spectroscopy with terahertz beams of dielectrics and semiconductors. *Journal of the Optical Society of America B*, **7** (10), 2006.
120. Petzelt, J., Kamba, S., Kozlov, G.V., and Volkov, A.A. (1996) Dielectric properties of microwave ceramics investigated by infrared and submillimetre spectroscopy. *Ferroelectrics*, **176** (1), 145–165.
121. Rupprecht, G. and Bell, R.O. (1962) Microwave losses in strontium titanate above the phase transition. *Physical Review*, **125** (6), 1915–1920.
122. Silverman, B.D. (1962) Microwave absorption in cubic strontium titanate. *Physical Review*, **125** (6), 1921–1930.
123. Kamba, S., Petzelt, J., Buixaderas, E., *et al.* (2001) High frequency dielectric properties of $A_5B_4O_{15}$ microwave ceramics. *Journal of Applied Physics*, **89** (7), 3900.
124. Zurmühlen, R., Petzelt, J., Kamba, S., *et al.* (1995) Dielectric spectroscopy of $Ba(B_{1/2}'B_{1/2}')O_3$ complex perovskite ceramics: correlations between ionic parameters and microwave dielectric properties. I. Infrared reflectivity study (1012–1014 Hz). *Journal of Applied Physics*, **77** (10), 5341.
125. Zurmühlen, R., Petzelt, J., Kamba, S., *et al.* (1995) Dielectric spectroscopy of $Ba(B_{1/2}'B_{1/2}')O_3$ complex perovskite ceramics: correlations between ionic parameters and microwave dielectric properties. II. Studies below the phonon eigenfrequencies (102–1012 Hz). *Journal of Applied Physics*, **77** (10), 5351.
126. Petzelt, J. and Setter, N. (1993) Far infrared spectroscopy and origin of microwave losses in low-loss ceramics far infrared spectroscopy in low loss ceramics. *Ferroelectrics*, **150** (1), 89–102.
127. Fukuda, K., Kitoh, R., and Awai, I. (1995) Microwave characteristics of mixed phases of $BaTi_4O_9$–$BaPr_2Ti_4O_{12}$ ceramics. *Journal of Materials Science*, **30** (5), 1209–1216.
128. Ferreira, V.M., Baptista, J.L., Kamba, S., and Petzelt, J. (1993) Dielectric spectroscopy of $MgTiO_3$-based ceramics in the 109–1014 Hz region. *Journal of Materials Science*, **28** (21), 5894–5900.
129. Petzelt, J., Pačesová, S., Fousek, J., *et al.* (1989) Dielectric spectra of some ceramics for microwave applications in the range of 1010–1014 Hz. *Ferroelectrics*, **93** (1), 77–85.

130. Tagantsev, A.K., Sherman, V.O., Astafiev, K.F., Venkatesh, J., and Setter, N. (2003) Ferroelectric materials for microwave tunable applications. *Journal of Electroceramics*, **11** (1/2), 5–66.
131. Subbaswamy, K.R. and Mills, D.L. (1986) Theory of microwave absorption in wide-band-gap insulators: the role of thermal phonon lifetimes. *Physical Review B*, **33** (6), 4213–4220.
132. Tagantsev, A.K., Petzelt, J., and Setter, N. (1993) Relation between intrinsic microwave and submillimeter losses and permitivity in dielectrics. *Solid State Communications*, **87**, 1117–1120.
133. Petzelt, J. and Kamba, S. (2003) Submillimetre and infrared response of microwave materials: extrapolation to microwave properties. *Materials Chemistry and Physics*, **79** (2–3), 175–180.
134. Wakino, K. (1996) Miniaturization techniques of microwave components for mobile communications systems: using low loss dielectrics. IEICE Technical Report, *Microwaves*, *The Institute of Electronics, Information and Communication Engineers*, **96** (26), 7–14.
135. Mollá, J., González, M., Vila, R., and Ibarra, A. (1999) Effect of humidity on microwave dielectric losses of porous alumina. *Journal of Applied Physics*, **85** (3), 1727.
136. Schlömann, E. (1964) Dielectric losses in ionic crystals with disordered charge distributions. *Physical Review*, **135** (2A), A413–A419.
137. Li, L. and Chen, X.M. (2014) Frequency-dependent *Qf* value of microwave dielectric ceramics. Jantunen, H. (ed.), *Journal of the American Ceramic Society*, **97** (10), 3041–3043.
138. Silva, M.A.S., Fernandes, T.S.M., and Sombra, A.S.B. (2012) An alternative method for the measurement of the microwave temperature coefficient of resonant frequency (τ_f). *Journal of Applied Physics*, **112** (7), 074106.
139. Tao, S., Zaki, K.A., and Chi, W. (2000) Tunable dielectric resonators with dielectric tuning disks. *IEEE Transactions on Microwave Theory and Techniques*, **48** (12), 2439–2445.
140. Felix, H.G. and Martinez, J.P. (1985) Analysis of dielectric resonators with tuning screw and supporting structure. *IEEE Transactions on Microwave Theory and Techniques*, **33** (12), 1453–1457.
141. Chen, S.-W., Zaki, K.A., and West, R.G. (1990) Tunable, temperature-compensated dielectric resonators and filters. *IEEE Transactions on Microwave Theory and Techniques*, **38** (8), 1046–1052.
142. Poplavko, Y.M., Prokopenko, Y.V., Molchanov, V.I., and Dogan, A. (2001) Frequency-tunable microwave dielectric resonator. *IEEE Transactions on Microwave Theory and Techniques*, **49** (6), 1020–1026.
143. Petrov, P.K. and Alford, N.M. (2001) Tunable dielectric resonator with ferroelectric element. *Electronics Letters*, **37** (17), 1066.